Physica Medica 133 (2025) 104978

Contents lists available at ScienceDirect

Physica Medica

journal homepage: www.elsevier.com/locate/ejmp

Review paper

Leveraging deep learning for improving parameter extraction from perfusion MR images: A narrative review

Elisa Scalco [a], Giovanna Rizzo [b], Nicola Bertolino [c,d], Alfonso Mastropietro [b,*]

[a] Istituto di Tecnologie Biomediche, Consiglio Nazionale delle Ricerche, Segrate, Italy
[b] Istituto di Sistemi e Tecnologie Industriali Intelligenti per il Manifatturiero Avanzato, Consiglio Nazionale delle Ricerche, Milano, Italy
[c] Department of Radiology, Northwestern University, Chicago, IL, USA
[d] Charles River Laboratories, Mattawan, MI 49071, USA

ARTICLE INFO

Keywords:
Perfusion MRI
Deep learning
DCE
DSC
ASL
IVIM
Parameter quantification

ABSTRACT

Background: Perfusion magnetic resonance imaging (MRI) is a non-invasive technique essential for assessing tissue microcirculation and perfusion dynamics. Various perfusion MRI techniques like Dynamic Contrast-Enhanced (DCE), Dynamic Susceptibility Contrast (DSC), Arterial Spin Labeling (ASL), and Intravoxel Incoherent Motion (IVIM) provide critical insights into physiological and pathological processes. However, traditional methods for quantifying perfusion parameters are time-consuming, often prone to variability, and limited by noise and complex tissue dynamics.

Recent advancements in artificial intelligence (AI), particularly in deep learning (DL), offer potential solutions to these challenges. DL algorithms can process large datasets efficiently, providing faster, more accurate parameter extraction with reduced subjectivity.

Aim: This paper reviews the state-of-the-art DL-based techniques applied to perfusion MRI, considering DCE, DSC, ASL and IVIM acquisitions, focusing on their advantages, challenges, and potential clinical applications.

Main findings: DL-driven methods promise significant improvements over conventional approaches, addressing limitations like noise, manual intervention, and inter-observer variability. Deep learning techniques such as convolutional neural networks (CNNs), recurrent neural networks (RNNs), and generative adversarial networks (GANs) are particularly valuable in handling spatial and temporal data, enhancing image quality, and facilitating precise parameter extraction.

Conclusions: These innovations could revolutionize diagnostic accuracy and treatment planning, offering a new frontier in perfusion MRI by integrating DL with traditional imaging methods. As the demand for precise, efficient imaging grows, DL's role in perfusion MRI could significantly improve clinical outcomes, making personalized treatment a more realistic goal.

1. Introduction

Perfusion magnetic resonance imaging (MRI) is a powerful non-invasive imaging technique that plays a pivotal role in the quantitative assessment of tissue microcirculation and perfusion dynamics. By probing the movement of contrast agents or endogenous spins, Perfusion MRI provides invaluable insights into various physiological and pathological processes, such as angiogenesis, blood–brain barrier disruption, tumor characterization, and neurovascular disorders. Different perfusion MRI techniques, such as Dynamic Contrast-Enhanced (DCE), Dynamic Susceptibility Contrast (DSC), Arterial Spin Labeling (ASL), and Intravoxel Incoherent Motion (IVIM), have emerged as essential tools in both clinical research and routine clinical practice [1].

While Perfusion MRI has proven to be an invaluable imaging technique, its full potential in clinical practice may be limited by the complexity of the accurate extraction of perfusion parameters from the acquired data. The interpretation and quantification of perfusion data remain inherently challenging due to the complexity of tissue perfusion processes, the confounding effects of noise, and the inherent limitations of conventional data analysis methods. Traditional analysis methods often require manual input, are time-consuming, and can be prone to inter- and intra-observer variability, which may hinder the

* Corresponding author at: Istituto di Sistemi e Tecnologie Industriali Intelligenti per il Manifatturiero Avanzato, Consiglio Nazionale delle Ricerche, via Alfonso Corti, 12, 20133 Milano, Italy.
E-mail address: alfonso.mastropietro@cnr.it (A. Mastropietro).

https://doi.org/10.1016/j.ejmp.2025.104978
Received 30 October 2024; Received in revised form 28 February 2025; Accepted 4 April 2025
Available online 11 April 2025

reproducibility and reliability of results [2].

Recently, the rapid advancements in deep learning (DL) techniques have revolutionized various fields of medical imaging. The unparalleled ability of DL algorithms to identify patterns, learn from vast datasets, and make predictions has stimulated widespread interest in their application to Perfusion MRI analysis. DL-based methods offer the potential to overcome the limitations of traditional approaches, enhancing the accuracy and precision of parameter extraction while reducing computational times, subjectivity and inter-observer variability.

As the demand for more precise and efficient quantification grows, the integration of DL methodologies presents a promising avenue to overcome these challenges. By harnessing the power of DL-driven parameter extraction, we can unlock a new era of Perfusion MRI applications, where rapid and precise assessment of tissue perfusion becomes attainable, facilitating better diagnosis, treatment planning, and monitoring of various pathological conditions.

In this paper, we present a comprehensive review of the state-of-the-art approaches that exploit the power of DL for the extraction of perfusion parameters from MRI data. Recent reviews on this topic have discussed the current status of compartment models in contrast-based perfusion MRI, without specific insights on DL-based methods for parameters quantification [3], or have favored a broader description of DL approaches in the clinical context, not limited to parameters estimation [4]. In both cases, IVIM model was not included in the reviews. In our study, we aim to highlight the advantages, challenges, and potential applications of these innovative techniques in the context of DCE, DSC, ASL, and IVIM perfusion MRI, with a specific focus on the quantification of parametric maps. Additionally, we discuss the implications of DL-driven parameter extraction for clinical decision-making, with an eye towards novel strategies to enhance explainability, data sharing and privacy.

The paper is structured as follows: In Section 2, we describe the theoretical foundations of DL techniques, elucidating their relevance to the complexities of Perfusion MRI data analysis. Section 3 offers a comprehensive survey of perfusion MRI models, with mathematical formulations for DCE, DSC, ASL and IVIM. Section 4 is focused on the presentation of recent DL-based methodologies proposed for parameter extraction in perfusion MRI, that we found in the searched literature. Section 5 emphasizes the specific advantages and limitations of the current approaches, highlights challenges and introduces future perspectives.

This review will not only serve as a reference for researchers and clinicians seeking a comprehensive understanding of DL-driven perfusion parameter extraction but also inspire further advancements in the field. By exploring the vast potential of DL in refining perfusion MRI analysis, we envision a future where improved diagnostic accuracy, personalized treatment planning, and enhanced patient outcomes become attainable realities.

2. Deep learning techniques

DL is generally considered a more advanced implementation of Machine Learning (ML) and it offers promising opportunities for fast and efficient imaging analysis [5]. ML represents a large field of research in the Artificial Intelligence (AI) context, thanks to the ability of learning model from data, by automatically identifying complex and high-dimensional patterns in existing datasets and making predictions or classifications based on new unseen data [6].

ML algorithms can be further subdivided into two broad categories, supervised and unsupervised learning [7]. Supervised learning refers to techniques in which a model is trained on inputs with known outcomes (labels). Once the algorithm is trained, it can make outcome predictions when applied to new data. In unsupervised learning, the algorithm has no access to the labels of the data but it is designed to learn on its own, finding undefined patterns or clusters within the dataset.

In medical imaging, Artificial Neural Networks (ANNs) – which are the backbone of DL – are the simplest architectures, derived from multilayers perceptron (MLP), where input data are mapped into global features through fully connected layers (Fig. 1A) [8]. DL uses biologically inspired ANNs to learn from large amounts of data and perform complex tasks [9] and one of the main differences between DL and ML is the ability of DL to independently learn abstract, high-order features from data without requiring feature selection. Typically, DL models consist of multiple layers of nonlinear units that process input data and produce output [10].

In the context of DL for medical image analysis, convolutional neural networks (CNNs) are exploited since they can capture the spatial structure and local patterns of image pixels. CNNs consist of multiple convolutional layers that apply filters to generate feature maps, followed by pooling layers that reduce dimensionality and increase feature invariance. The final fully connected layer connects every neuron in one layer to every neuron in the next layer, and perform classification or regression tasks based on the extracted features (Fig. 1B) [11].

A particular type of CNN primarily designed for image segmentation is the U-Net model, introduced by Ronneberger et al. [12]. It is characterized by the typical U-shaped architecture, consisting of a contracting (encoder) path that captures the context in the image by progressively reducing the spatial dimensions through convolutional and pooling layers, and an expansive (decoder) path that reconstructs the image's spatial dimensions through upsampling and convolutional layers. The other relevant key characteristic is the presence of skip connections between corresponding layers in the encoder and decoder paths, which allow the model to combine high-resolution features from the contracting path with the upsampled features in the expansive path (Fig. 1B).

Autoencoders are a type of ANN or CNN used to learn efficient coding of unlabeled data through unsupervised learning [13]. They are composed of an encoder, which compresses the input into a latent-space representation, and a decoder, which reconstructs the input from this representation (Fig. 1C). Autoencoders are typically used for dimensionality reduction, feature learning, and generative modeling.

A different type of DL framework is given by Generative Adversarial Networks (GANs), which are designed for generating realistic synthetic data. Introduced by Ian Goodfellow and his colleagues in 2014, GANs consist of two neural networks, a generator and a discriminator, that are trained simultaneously through an adversarial process (Fig. 1D) [14]. One of the most adopted GAN models is represented by Pix2Pix, which is a type of image-to-image translation algorithm based on conditional GAN, aiming at transferring an image across different domains from one to another. Specifically, the generator processes the source image as input and attempts to create an image that closely resembles the target image. Meanwhile, the discriminator evaluates both the generated image and the actual target image from the dataset, determining how likely the generated image is to be authentic. Through this iterative process, the generator and discriminator continuously refine their performance, leading to progressively improved results. These types of networks have been widely employed in medical imaging, especially for the generation of images with enhanced quality or with different MRI contrast.

In recent years, stable diffusion models have gained attention in the context of image synthesis, including medical applications, by integrating language and image processing models. These models can generate high-quality and realistic images from text prompts across various domains, with the most advanced approach represented by the text-guided diffusion model GLIDE [15,16].

Recurrent Neural Networks (RNNs) are a class of neural networks designed for sequential data. Unlike traditional neural networks, RNNs have connections that form directed cycles, enabling them to maintain a hidden state that can capture information about previous steps in the sequence (Fig. 1E) [13]. This makes them particularly effective for tasks like time series prediction, natural language processing (NLP), and any application where temporal dynamics are important, such as DCE- and

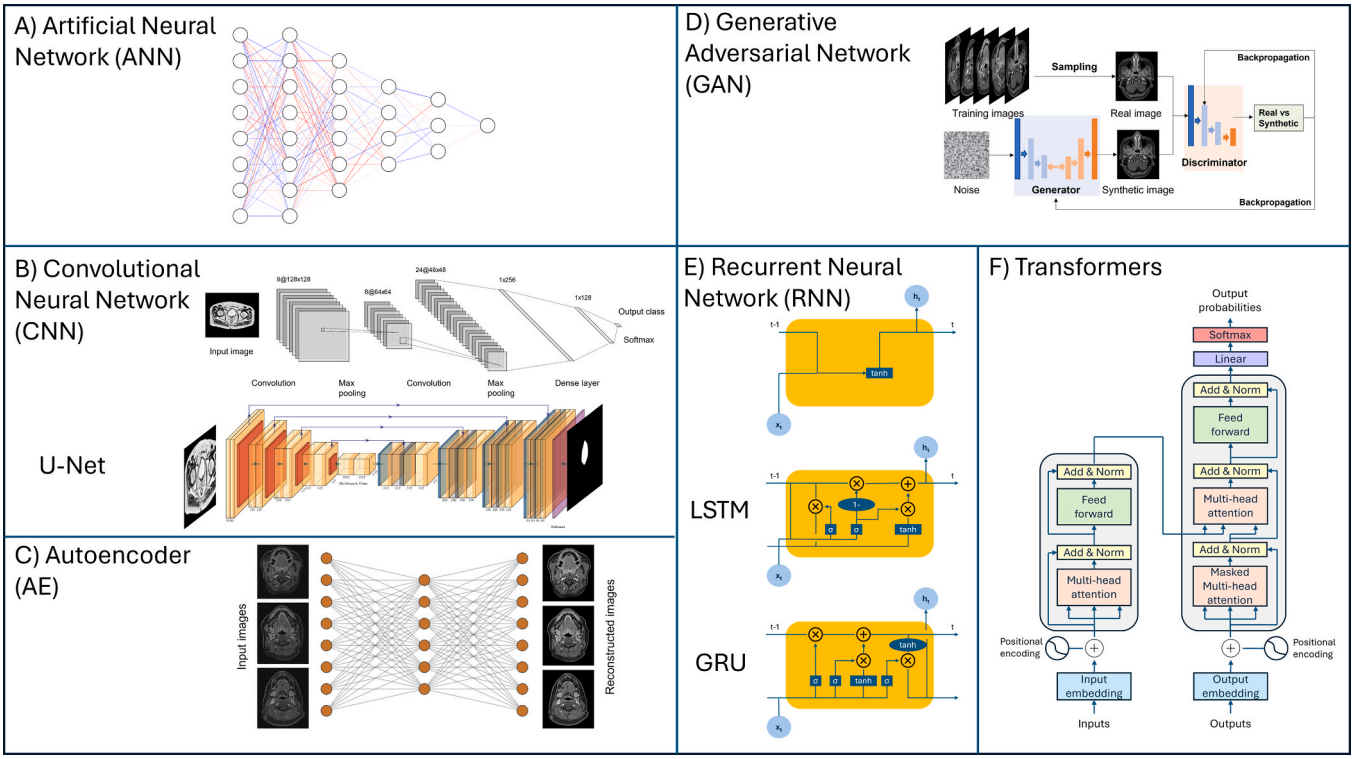

Fig. 1. Schematic representation of the main architectures for DL models.

DSC-MRI. Long Short-Term Memory (LSTM) networks are a special kind of RNNs designed to better capture long-range dependencies and mitigate the vanishing gradient problem [17]. LSTMs have a more complex structure than standard RNNs, featuring three gates, which control the flow of information (Fig. 1E). This gating mechanism allows LSTMs to maintain and update a cell state, which acts as a memory, over long sequences, making them particularly useful for tasks like language modeling, speech recognition, and time-series prediction. Gated Recurrent Unit (GRU) networks are another type of RNN designed to address the vanishing gradient problem and capture long-term dependencies, similar to LSTMs but with a simpler architecture, which allows to perform similarly to LSTMs while being computationally more efficient (Fig. 1E) [18].

Transformers are a type of neural network architecture designed to handle sequential data with greater efficiency and effectiveness than traditional RNNs or LSTMs. Introduced by Vaswani et al. in 2017, transformers rely entirely on a mechanism called self-attention to process input data, allowing for greater parallelization and improved handling of long-range dependencies [19]. Key components of the transformer architecture include: i) the Self-Attention Mechanism, which allows the model to weigh the importance of different tokens in the input sequence when making predictions; ii) Positional Encoding, to retain information about the position of each token in the sequence; iii) Multi-Head Attention, which allows the model to focus on different parts of the sequence simultaneously and capture diverse aspects of the data (Fig. 1F). Transformers have revolutionized NLP and are the foundation of many state-of-the-art models. The transformer architecture has also been adapted for other domains, such as image processing (Vision Transformers) and time-series forecasting, showcasing its versatility and effectiveness across various types of data.

Recent advancements in DL for medical imaging, particularly regarding Perfusion MRI, include novel learning techniques. Beside supervised and unsupervised learning, physics-informed learning has been introduced as an approach that integrates physical laws and constraints directly into the learning process. This method enhances the training and prediction capabilities of models, by ensuring that the learned solutions adhere to known physical principles. Physics-informed learning bridges the gap between traditional scientific modeling and modern machine learning, resulting in models that are both powerful and grounded in reality. In the estimation of perfusion coefficients, this approach can be adopted by considering pharmaco-kinetic models that describe the concentration curves of contrast agents, or mathematical models related to the dynamics of MR signal intensity. Specific details will be given in the next section for each perfusion technique.

3. Perfusion MRI models

3.1. DCE-MRI

DCE-MRI is a functional imaging technique for the depiction of in-vivo tissue perfusion. It is widely employed to study non-invasively the integrity of the vascular system of different organs like heart, kidney, liver, prostate and brain, gaining insights on pathogenesis and therapies response in the research of a whole pool of pathologies [20]. To perform DCE-MRI an exogenous contrast agent (CA) is injected in the bloodstream during the acquisition of a time series of T1-weighted images. Images intensity will change proportionally to the concentration of CA present in the tissue and from the concentration curve over time it is possible to extract valuable blood perfusion information. While it is possible to run a trivial nonparametric analysis on the time series looking at the signal intensity over time, the results provided by such analysis are non-quantitative and they don't derive physiological information. On the other hand, a parametric analysis fits pharmacokinetic (PK) models to the dynamically acquired concentration curves providing quantitative tissue parameters related to vascularity (e.g. permeability and volume fractions). Perfusion coefficients derived from PK models can be computed from a single organ by considering the time-series signal averaged over the region of interest (ROI), or voxel-wise to obtain quantitative parametric maps. The PK model mostly used is the Extended Tofts-Kety (ETK) model [21] expressed in the following equation:

$$C_t(t|\theta) = v_p C_p(t) + v_e k_{ep} \int_0^t C_p(\tau) e^{-k_{ep}(t-\tau)} d\tau \quad (1)$$

Where $\theta = \{v_p, v_e, k_{ep}\}$, C_t is the CA concentration at the equilibrium, $C_p(t)$ is the blood plasma CA concentration in the input artery over time, also known as Arterial Input Function (AIF), v_p and v_e are the relative volumes of blood plasma and extra-vascular-extra-cellular space (EES), k_{ep} represents the rate constant for efflux of CA back into plasma from the tissue EES. The last ETK coefficient not directly present in the equation is K^{trans} that represents the volume transfer constant that influences the degree of contrast enhancement, which is equal to $v_e \times k_{ep}$ [2].

Another popular PK model frequently adopted in the quantification of DCE-MRI perfusion maps is the Patlak model, which can be considered as a special case of the ETK model, where the backflux from the EES into the blood plasma compartment is negligible [22]. In this case, K^{trans} and v_p are the only parameters θ to be estimated from the following equation:

$$C_t(t|\theta) = v_p C_p(t) + K^{trans} \int_0^t C_p(\tau) d\tau \quad (2)$$

For a comprehensive and detailed description of the models and methods available for analyzing DCE-MRI, the readers are encouraged to refer to specific reviews [20].

3.2. DSC-MRI

Dynamic Susceptibility Contrast MRI (DSC-MRI) uses a paramagnetic gadolinium-based CA, which diffuses through microvasculature and causes magnetic field inhomogeneities around blood vessels, accelerating proton dephasing in the surrounding tissue and consequently a T2* signal loss. The signal intensity during the rapid passage of the injected CA bolus through the tissue is typically acquired with EPI sequences able to characterize the transient MR signal drop with adequate temporal resolution.

The relation between MRI signal intensity $S(t)$ and CA tissue concentration $C_t(t)$ is described by Eq. (3)

$$C_t(t) = -\frac{k}{TE} \ln\left(\frac{S(t)}{S(0)}\right) \quad (3)$$

Where $S(0)$ is the baseline intensity, and k is a proportionality constant depending on the tissue, the CA, the field strength and the pulse sequence parameters.

From the concentration–time curve $C_t(t)$, parameters characterizing the tissue perfusion status, such as cerebral blood volume (CBV), cerebral blood flow (CBF), mean transit time (MTT), time to peak (TTP), time to max (T_{max}), can be estimated by applying traditional tracer kinetic models for intravascular agents [23]. In particular, CBV can be calculated as:

$$CBV = \frac{\int C_t(t) dt}{\int C_a(t) dt} \quad (4)$$

Where $C_a(t)$ is the CA concentration curve of the feeding artery corresponding to AIF. To calculate the other parameters CBF, MTT, and T_{max}, it is necessary the estimation of the residue function R_t, which is then convolved with AIF, as expressed in the following equation:

$$C_t(t) = CBF \times R_t(t) \otimes C_a(t) \quad (5)$$

Where the symbol $\times$ indicates multiplication and the symbol $\otimes$ refers to convolution; $CBF \times R_t$ represents the tissue response function related to the tissue hemodynamic status [24]. Finally, the estimation of CBF, MTT and T_{max} relies on the following relations:

$$CBF = \max(CBF \times R_t) \quad (6)$$

$$MTT = FWHM(R_t) \quad (7)$$

$$T_{max} = argmax(R_t) \quad (8)$$

However, $CBF \times R_t$ can be acquired by deconvolution with the AIF, which is a typical ill-conditioned operation, based on nonlinear models applied to noisy measurement data, requiring strong regularization [25].

3.3. ASL-MRI

Arterial spin labeling (ASL) is a noninvasive technique used to measure blood flow in the tissue by using magnetically labeled water protons from arterial blood as an endogenous tracer. ASL has been used for various clinical and research purposes and can provide valuable information about tissue perfusion that may complement other MRI modalities [26,27].

ASL is based on the acquisition of two paired images: labeled (or spin labeled) – those including signal from both labeled water and static tissue water – and control (or spin-unlabeled). During the ASL preparation module, labeled images are obtained using a radiofrequency pulse to invert the magnetization of the arterial blood below the imaging slab. Conversely, to collect the control images, no labeling is performed. After spin labeling and the post labeling delay (PLD) time, MR images with or without spin labeled can be acquired with different common pulse sequences. The difference between such labeled and control images reflects the amount of labeled blood delivered to the tissue by perfusion [28,29].

The magnetization difference collected after a single-PLD ASL acquisition is typically fitted to a kinetic model to get the cerebral blood flow (CBF), using the convolution integral [30]:

$$\Delta M(t) = 2 \bullet M_{0,a} \bullet CBF \bullet \int_0^t c(t) \bullet r(t-\tau) \bullet m(t-\tau) d\tau \quad (9)$$

Where $M_{0,a}$ is the equilibrium magnetization in a blood-filled voxel, $c(t)$ is the delivery function or fractional AIF, and $r(t-\tau)$ is the residue function that describes the fraction of labeled spins arriving at a voxel at time τ that still remains within the voxel at time t. The magnetization relaxation term $m(t-\tau)$ quantifies the longitudinal magnetization fraction of labeled spins arriving at the voxel at time τ that remains at time t [31]. The delivery function $c(t)$ can be traditionally expressed as:

$$c(t) = \begin{cases} 0, & t < ATT \\ e^{-t \bullet R_{1a}}, & ATT \le t < \tau_d \\ 0, & t \ge \tau_d \end{cases} \quad (10)$$

Where ATT is the arterial transit time, τ_d is the time for the trailing edge of the labeled blood bolus to reach the tissue, and R_{1a} is the longitudinal relaxation rate of arterial blood.

As a more reliable alternative, multiple-PLD ASL, consisting in repeated ASL acquisitions with different PLDs, can be used to quantify CBF and ATT.

3.4. IVIM-MRI

IntraVoxel Incoherent Motion (IVIM) is a type of Diffusion-weighted MRI (DW-MRI), firstly proposed in the 80′s by Le Bihan to simultaneously estimate diffusion and perfusion tissue properties [32]. In this technique, the MR signal in each voxel is modeled by a bi-exponential decay over the *b-values*, in which the first fast component describes water diffusion related to tissue perfusion (blood flow in the capillaries), and the second slower component is associated to molecular diffusion in tissues. The bi-exponential descriptors are the true diffusion coefficient D, the pseudo-diffusion coefficient related to perfusion D* and the perfusion fraction f, expressed in the following equation:

$$S(b) = S_0\left(fe^{-bD^*} + (1-f)e^{-bD}\right) \quad (11)$$

Where *S(b)* is the signal intensity at the different *b-values* and S_0 is the non-diffusion dependent signal intensity.

3.5. Factors influencing perfusion parameters quantification

Multiple MRI acquisition factors influence perfusion parameter quantification including spatial resolution, signal-to-noise ratio (SNR), partial volume effects, and pulse sequence protocols. Furthermore, perfusion MRI models based on dynamic acquisitions, such as DCE, DSC and ASL, are also highly dependent on temporal resolution.

This is particularly relevant for the estimation of AIF in the DCE and DSC models, which is necessary for a correct and precise quantification of PK parameters. AIF represents the temporal variations in contrast agent concentration within a blood vessel supplying the tissue of interest. The AIF typically exhibits a rapid uptake, a brief peak phase, and a prolonged washout period, with kinetics distinct from those of surrounding tissues. The manual selection of the AIF is often impractical [33], and achieving a precise estimation of both the AIF and PK coefficients requires a sufficiently high temporal resolution, which, however, may come at the expense of spatial resolution and SNR [20].

Regarding ASL, its inherently low temporal resolution makes it difficult to acquire abundant temporal information with sufficient SNR in a clinical setting. To address this issue, researchers have worked to improve and optimize the bolus design of multi-delay ASL, through a robust ATT estimation strategy, the signal weighted-delay (WD) method [34]. It avoids using Non-Linear Least Squares (NLLS) fitting, which, on the contrary, has still remained the standard method to estimate CBF.

Finally, the quantification of the IVIM model parameters, which typically does not rely on a time-dependent acquisition, requires to correctly sample the bi-exponential signal decay, by acquiring different *b-values*. The optimal choice of *b-values* sampling should be carefully planned, considering that micro-perfusion contribution vanishes at *b* larger than a certain threshold (generally chosen at 200 s/mm^2) [35], and that it is also dependent on the type of tissue or organs to be examined. The dependence of IVIM parameter quantification on this factor has been explored in several works [36–39].

4. Deep learning in perfusion MRI

4.1. DCE-MRI

One of the most adopted methods to quantify DCE parameters is the

Table 1
List of papers proposing the use of DL approaches for DCE-MRI applications.

Task	Type of DL method	Data	Validation	Evaluation metrics	Code available	Ref
Two compartments filtration model (2CFM) quantification	ANN – Supervised	Simulations + 10 healthy subjects (kidneys)	Internal by split	MAPE < 15 % $R^2 > 0.8$	No	[40]
ETK and Patlak model quantification	CNN – Supervised	15 stroke patients (preospective)	Leave-one-subject-out	nRMSE = 1.64 SSIM = 0.97	No	[41]
ETK model quantification	CNN – Supervised	Simulations + 24 brain tumor patients (prospective)	Internal by split	CCC > 0.986 (K^{trans}) CCC > 0.965 (v_p) CCC > 0.948 (v_e)	Yes	[42]
ETK model quantification	CNN – Supervised	19 brain tumor patients (retrospective)	Internal by split	Bland-Altman plots	No	[43]
ETK and Patlak model quantification	GANs – Unpaired, physics-informed	Simulations + 116 brain tumor patients + 232 MCI and normal subjects	Internal by split	Avg PSNR = 39.76 dB Avg SSIM = 0.973	No	[44]
ETK model quantification	CNN – Supervised + uncertainty quantification	Simulations + 3 brain tumor patients (retrospective)	On simulated digital objects	RMSE < 0.07 Max error < 0.25	No	[45]
Patlak model quantification	2.5D UNet – Unsupervised	10 breast + 19 brain cancer patients (public datasets)	Internal by split + cross-validation	PSNR = 40.21 dB SSIM = 0.95 (K^{trans}) PSNR = 28.69 dB SSIM = 0.78 (v_p)	Yes	[46]
Patlak model quantification	UNet – Hybrid approach	10 breast + 19 brain + 22 prostate cancer patients (public datasets)	Internal by split	Improvement in PSNR up to 3 dB	Yes	[47]
ETK model quantification	LSTM-based – Supervised	Simulations + 103 head-and-neck cancer patients (retrospective)	Internal by split	NRMSE = 1.36 (K^{trans}) NMRSE = 1.14 (v_e) NMRSE = 0.97 (v_p)	No	[48]
ETK model quantification	GRU with attention layers – Unsupervised, physics-informed	Simulations + 28 pancreatic cancer patients (retrospective)	Internal by split	Random errors and SSIM from GRU better than other approaches	Yes	[2]
Toft model quantification + MR Dispersion Imaging	Transformer – Two-stage estimation	Simulations + 182 prostate cancer patients (retrospective)	On simulated digital objects	Fitting error reduction compared to other approaches	No	[49]
AIF estimation	Pix2Pix – Adversarial learning	386 astrocytoma patients (retrospective)	Internal by split	Avg AUC = 0.83 Avg ICC = 0.82	Yes	[50]
Fully automated DCE-MRI analysis	UNet – CNN for segmentation + cubic model for AIF estimation	Simulations + Brain tumor patients (public dataset)	Cross-validation	Fitting error = 1.51 % (K^{trans}) Fitting error = 2.78 % (v_e)	No	[51]
DCE-MRI denoising	Ensemble of deep autoencoders	Simulations + 9 stroke patients (retrospective) + 24 brain cancer patients (retrospective and public database)	Training on simulations, testing on real data	Reduced MSE w.r.t. noisy and cleaned images compared to other approaches	No	[52]
DCE-MRI reconstruction	GANs – Adversarial learning	490 healthy brains + 19 MS patients (public databases) + 14 brain cancer patients (retrospective)	Internal by split	PSNR, SSIM and MSE better than other approaches	Yes	[53]

ETK: Extended Toft Model; ANN: Artificial Neural Network; CNN: Convolutional Neural Network; LSTM: Long-Short Term Memory; MS: Multiple Sclerosis; GANs: Generative Adversarial Networks; MAPE: Mean Absolute Percentage Error; nRMSE: normalized Root Mean Square Error; CCC: Concordance Correlation Coefficient; PSNR: Peak Signal-to-Noise Ratio; SSIM: Structural Similarity Index Measure; AUC: Area Under the Curve; ICC: Intraclass Correlation Coefficient.

NLLS approach, which results in large variance and bias parameter predictions and also requires a large amount of time [2]. Multiple research studies showed how DL algorithms can be employed to improve the results provided by the DCE approaching different critical aspects of this technique [4]. A schematic overview of the works employing DL in the context of DCE-MRI is reported in Table 1.

The first attempts of using DL approaches for DCE-MRI parameter quantification showed that the adoption of an ANN (Fig. 2) [40] or a CNN [41,42] can improve the accuracy and the speed in estimating PK model parameters compared to NLLS methods. These models were trained using simulated data or directly using real DCE-MRI acquisitions, and took as input the kinetic signal information. In the ANN framework, PK estimation is performed voxel-wise [40]; the use of CNN allowed voxel-wise parameter quantification by considering multiple time-series signals (original dynamic DCE signal and CA concentration in blood) [42], as well as the parametric map estimation by taking DCE image patch-time series as input [41]. Moreover, these works highlighted that DL-based modelling does not need the estimation of a patient-specific AIF to quantify PK coefficients with accuracy comparable to NLLS approaches, and to obtain clinical measurements derived from parametric maps in high agreement with blood tests. Nonetheless, the addition of AIF to the DCE-MRI time-series as input to the CNN can improve the prediction performances, as reported by Kettelcamp et al. [43]. The adoption of CNN has also the advantage of better generalizing the prediction in voxels belonging to the same tissues. Further improvements were highlighted by Oh et al., who proposed an unpaired method, based on physics-informed Cycle-GAN architecture, for the simultaneous estimation of PK model parameters and AIF, without relying on paired supervised learning [44]. In fact, the main limitation of supervised approaches is that they necessitate paired input DCE-MRI images and corresponding labeled PK parameter maps, which typically require time-consuming NLLS estimations, and which depend on the accuracy of AIF measurement. The evaluation based on a large dataset of 116 brain tumor patients and 232 Mild Cognitive Impairment (MCI) subjects demonstrated that the unpaired Cycle-GAN approach provided accurate PK quantification and reliable and high-quality AIF estimation. Another interesting work combined the use of CNN with Bayesian estimation to simultaneously predict PK model coefficients and quantify uncertainty from the posterior distribution over the physiological parameters, to give the confidence level for each pixel [45].

A key limitation of CNNs for PK parameter estimation is their reliance on temporal resolution being represented as multiple input channels, making them sensitive to variations in the temporal dimension. Furthermore, when AIF estimation is required, high temporal resolution is needed, often coming at the cost of reduced spatial resolution or prolonged acquisition times. These constraints hinder the generalizability of CNN-based models, as test data must maintain the same number of frames and sampling intervals as the training data to ensure consistent performance. A possible solution to this problem was given by the use of a 2.5D UNet, with the purpose of directly estimate PK

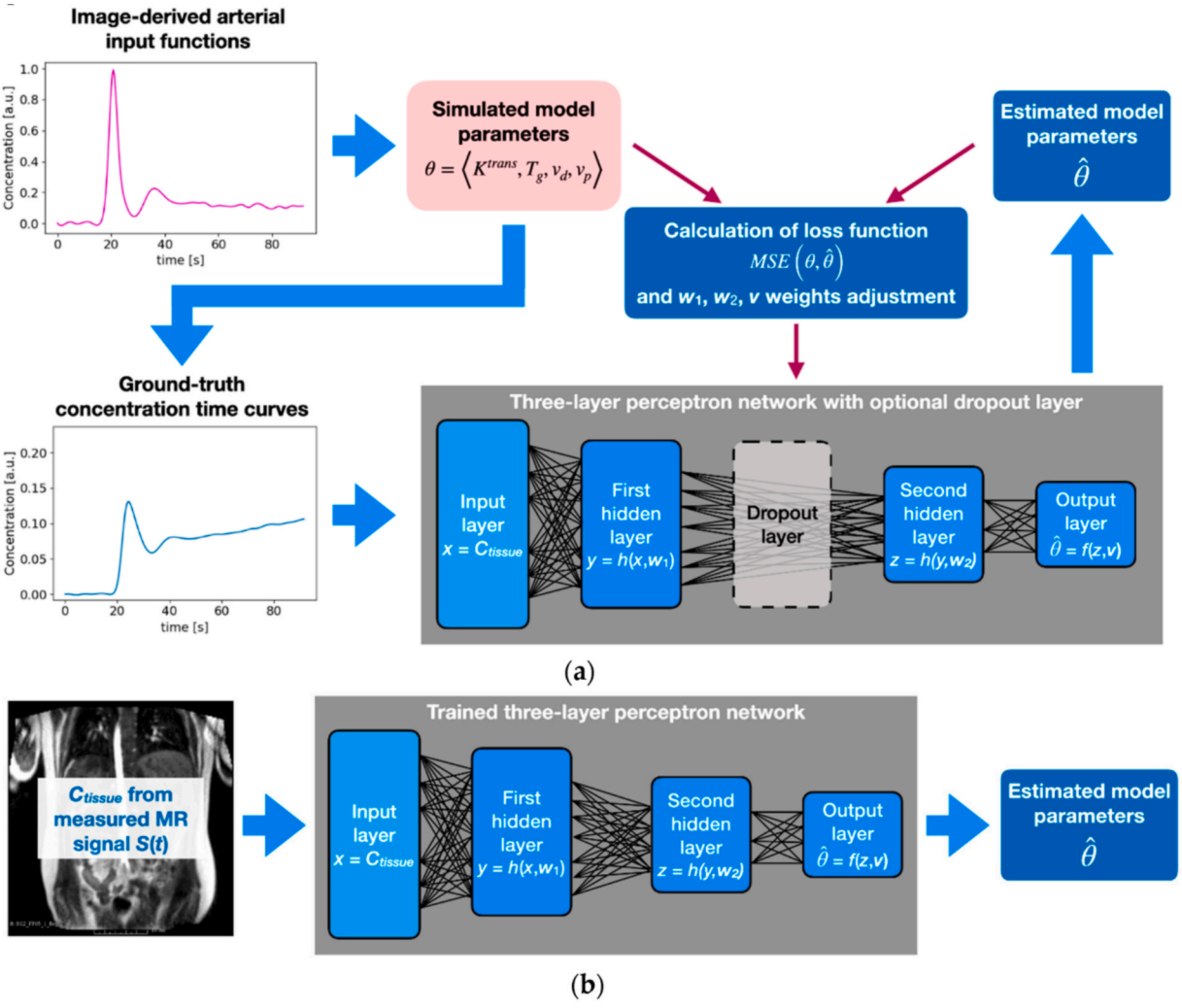

Fig. 2. Overview of a pharmacokinetic (PK) model parameter fitting using the artificial neural network proposed by Klepaczko et al., operating in the training (a) and recall (b) modes. Figure reproduced from Klepaczko et al., 2020, Appl. Sci., 10(16), 5525, under the Creative Commons license (CC-BY 4.0) [40].

coefficients from undersampled time-series DCE-MRI acquisitions to obtain a time-invariant network. In a recent work, the authors proposed a 2.5D UNet composed by 3D convolutional layers for the encoder part and 2D convolution layers for the decoder part [46]. The bottleneck consists of an averaging layer along the temporal axis to convert 3D data into 2D data. In this way, the network becomes invariant to changes in temporal and spatial dimensions while training and testing. This approach was proposed for temporally undersampled DCE-MRI acquisitions at different undersampling rates (8X, 12X and 20X) from breast and brain cancer patients, obtaining better peformances than networks requiring resampling, in terms of Peak Signal-to-Noise Ratio (PSNR) and Structural Similarity Index Measure (SSIM). However, the authors highlighted that the main limitation of this approach is that the network cannot generalize across different undersampling rates, and thus a new network has to be trained for each specific undersampling rate. In a next study, the same group proposed a novel strategy to overcome this problem, by proposing a hybrid approach for the direct estimation of DCE-MRI parameters, which combined iterative reconstruction models, able to adapt themselves to the number of time samples, and data-driven deep learning priors from PK models [47]. The adoption of pre-trained CNNs to estimate the priors brought substantial improvements in the direct parameters estimation, even with small datasets, compared to traditional iterative direct methods.

Nonetheless, to solve the limitation of the dependency from undersampling rate, RNNs seem to provide the best solution, as they are able to learn temporal relationships in sequential data. Among them, LSTM showed superior ability in mapping DCE-MRI time-curves compared to state-of-the-art CNNs and NLLS methods [48]. This was explained by the LSTM capability to extract dynamic features and temporal correlation in the signal intensity-time series of DCE-MRI, in contrast to CNNs, which extract spatial features from the DCE-MRI volumes but has a limited capability to exploit the temporal relationships in the data. Even better results were achieved by Ottens et al., who proposed the use of GRU RNNs combined with attention layers [2]. In fact, they obtained performance similar to LSTM, but with a fewer number of trainable parameters, which make this approach more attractive, generalizable and fast. Moreover, the introduction of attention layers can help the user to understand what the network is focusing on, thus increasing the explainability of the method. An illustrative example of the obtained parametric maps is shown in Fig. 3, where the results obtained by the GRU approach are compared with the standard NLLS method and with traditional CNN architectures. GRU showed less noisy maps compared to NLLS, and more reliable values compared to CNN and U-Net.

Finally, a two-stage estimation framework based on transformers was proposed to a fast modified MR Dispersion Imaging (mMRDI) model [49]. This model has been introduced to characterize the intravascular dispersion of contrast agent, and the parameters related to it can be included in the AIF estimation, to improve the precision in the estimation of PK parameters. The authors proposed a transformer-based neural network to perform a coarse estimation of the PK parameters, and then an iterative NLLS method to further refine the coarse estimation, which significantly speeds up and enhances the accuracy of PK modeling. They trained the network on simulations and validated on simulated digital objects and on a cohort of 182 retrospective prostate cancer patients, obtaining a reduction in fitting error compared to previous approaches and increased classification performances in discriminating clinically

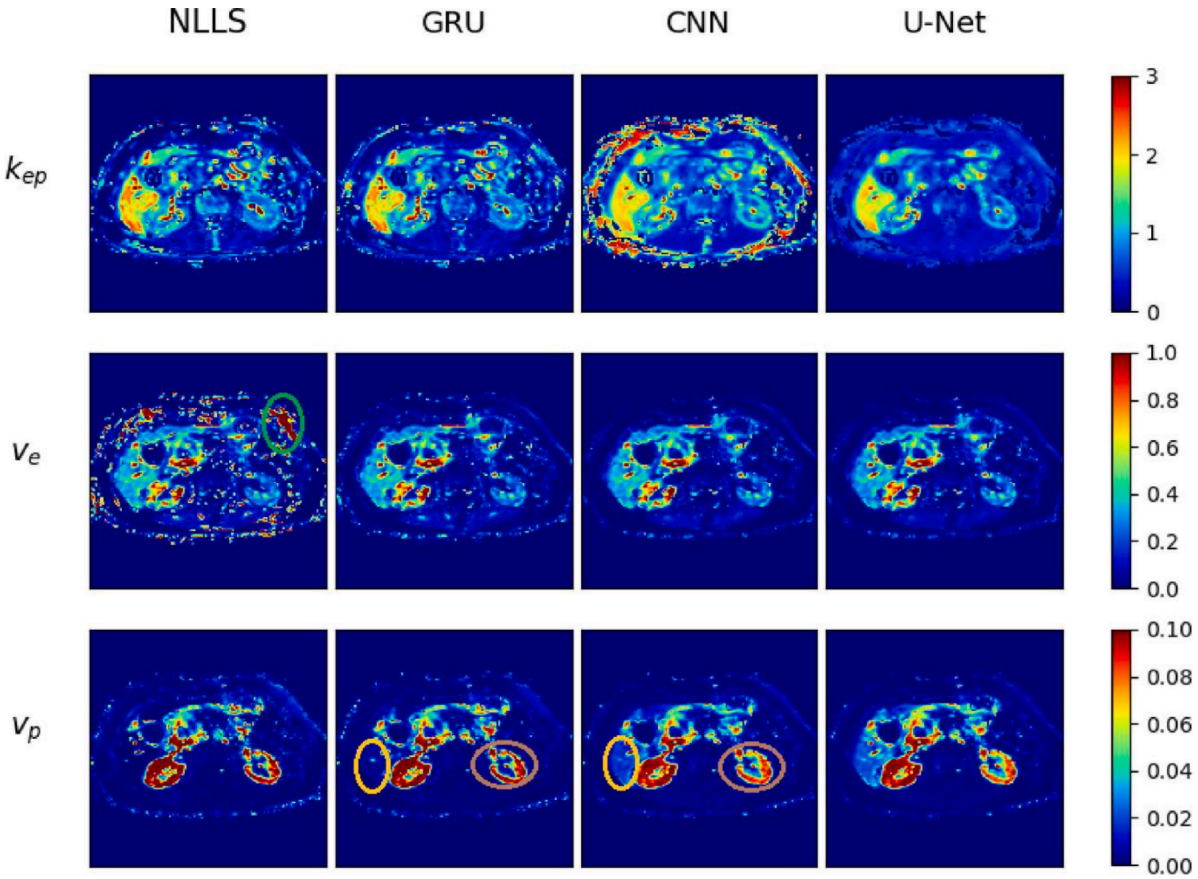

Fig. 3. Examples of DCE-MRI parameter maps obtained with the NLLS, GRU, CNN and U-Net methods. The GRU shows less noisy predictions on the v_e parameter than the NLLS method (green oval). The CNN shows noisy predictions on the border cases of the k_{ep} parameter while the U-Net shows a smooth parameter map but a lack of detail compared to the other methods. The CNN and U-Net also predict higher v_p values for the liver region (orange oval) and lower v_p values in the left kidney (brown oval) compared to the NLLS and GRU. Figure from Ottens et al., 2022, Med Imag Anal, 80, 102512, under the Creative Commons license (CC-BY 4.0) [2]. (For interpretation of the references to colour in this figure legend, the reader is referred to the web version of this article.)

significant prostate cancer from normal tissue.

Beside PK models fitting from DCE-MRI data, DL has been proposed also to improve other related aspects that can help in perfusion quantification. For example, two adversarial trained CNNs were proposed to obtain a reliable measurement of AIF, which is essential to derive a robust PK model, from an AIF extracted from a DSC acquisition [50]. DL was also proposed to provide an automatic workflow to pre-process and segment DCE-MRI for the extraction of perfusion parameters [51]. Furthermore, DL approaches were employed for image denoising and image enhancement. Benou et al. [52] proposed a DL neural network to improve SNR and reconstruction of the concentration curve without disrupting the original contrast quality and without assumption on the noise distribution. Shaul et al. [53] reconstructed a down sampled DCE MRI k-space mimicking a fast-imaging acquisition, using GANs.

4.2. DSC-MRI

In the recent years, model-free approaches based on DL have been proposed for the quantification of DSC parameters, with the purpose of both overcoming the limitations of model-based estimation and reducing computing time (see Table 2).

One of the first attempts in this direction was a bi-input convolutional neural network (bi-CNN) to estimate four perfusion parameters (CBV, CBF, MTT, T_{max}) starting from the signals of interest $C_t(t)$ and AIF (t), avoiding an explicit deconvolution method [54]. Results evaluated on a retrospective population of 11 stroke patients showed that the method produced good approximations for all parameters, with relative average root-mean-square error less than 5% of the maximum values. Furthermore, the estimated perfusion maps for quantifying the salvageable tissue volume in stroke agreed with ground truth for more than 80%.

With the same purpose of avoiding deconvolution, McKinley et al. compared different ML models (multiple regression, random forest, Support vector machine) and a standard feed forward neural network, for the estimation of DSC parameters from AIF and $C_t(t)$ [25]. They directly worked on the dynamic series of DSC images, voxel-by voxel, providing the quantitative DSC-derived perfusion maps as output. As major result, they found that Random Forest performed better, followed by the neural network; however, neural network appeared more robust with more reproducible results, as verified on phantom images.

Supervised deep learning applied to DSC raw images was proposed and validated on a dataset of 151 ischemic stroke patients [33]. The authors implemented a CNN to capture the temporal evolution of the raw perfusion sequence voxel-wise. The network architecture core was complemented with different "optional" pre or post processing blocks, aimed at solving specific issue, such as modeling of voxel spatial correlation, modeling injection bolus structure, introducing data augmentation to prevent learning a global bolus arrival time. Results showed good performance of the method in terms of mean absolute error with clipping (value ranging from 0.524 to 0.738), with the best result when only the additional augmentation block in used.

A two-encoder approach that first encodes the one-dimensional waveforms and then encodes the spatial information using a convolutional network with the U-Net architecture was recently proposed by Talebi et al. [55] (Fig. 4). The initial 1D encoder effectively incorporates information along the time dimension, whereas the U-Net architecture efficiently extract crucial features to generate CBV/CBF estimations. The authors found comparable performance to FDA-approved commercial software. The main advantage of this approach is that it implicitly incorporates the arterial input waveforms and venous output waveforms as inherent variables embedded within each 4D-dataset.

Recently, in an interesting review, Rotkopf et al [56] proposed RNNs as a very promising approach to learn quantitative maps from DSC data. The rationale for this choice relies on the good characteristics of these networks, which are natively designed for sequential input data, with a one-to-one-relationship between each temporal position in the input

Table 2
List of papers proposing the use of DL approaches for DSC-MRI applications.

Task	Type of DL method	Data	Validation	Evaluation metrics	Code available	Ref
DSC quantification	CNN – Supervised	11 stroke patients (retrospective)	Leave-one-patient-out cross-validation	RMSE = 4.80 ml/100 g (*CBV*); 27.4 ml/100 g/min (*CBF*); 1.18 s (*MTT*); 1.33 s (T_{max})	No	[54]
DSC quantification	CNN – Supervised	151 stroke patients (retrospective)	Internal by split	0.5 < MAEC < 0.8	No	[33]
DSC quantification	CNN – Supervised	159 patients with brain perfusion abnormalities (retrospective)	Internal by split	MAE = 1.91 ml/100 g/min; RMSE = 7.77 ml/100 g/min (*rCBF*); MAE = 0.59 ml/100 g; RMSE = 2.63 ml/100 g (*rCBV*)	No	[55]
DSC quantification	LSTM – Supervised	Brain subjects	Not specified	Not specified	No	[56]
DSC quantification	ANN – Physics-informed	Simulations + 20 stroke patients (retrospective)	Training on simulations, validation on simulations and patient data	MAE < 10 ml/100 g/min (*CBF*); MAE lower than other approaches for *MTT* and T_{max}	No	[24]
DSC quantification	ANN – Physics-informed	Simulations + 17 brain cancer patients (retrospective)	Training on simulations, validation on patient data	RMSE = 26.1 (*CBF*), 1.72 (*CBV*) ; SSIM = 0.91 (*CBF*), 0.98 (*CBV*) ; PSNR = 24.5 (*CBF*), 47.86 (*CBV*)	No	[57]
DSC quantification	CNN – Physics-informed	138 brain patients (retrospective)	Internal by split	SSIM = 0.95 (*CBV*), 0.94 (*CBF*), 0.86 (T_{max}); PSNR = 31.6 (*CBV*), 29.1 (*CBF*), 23.4 (T_{max})	Yes	[58]

CNN: Convolutional Neural Network; ANN: Artificial Neural Network; LSTM: Long-Short Term Memory; RMSE: Root Mean Square Error; MAEC: Mean Absolute Error by Clipping; SSIM: Structure Similarity Index Measure; PSNR: Peak Signal-to-Noise Ratio.

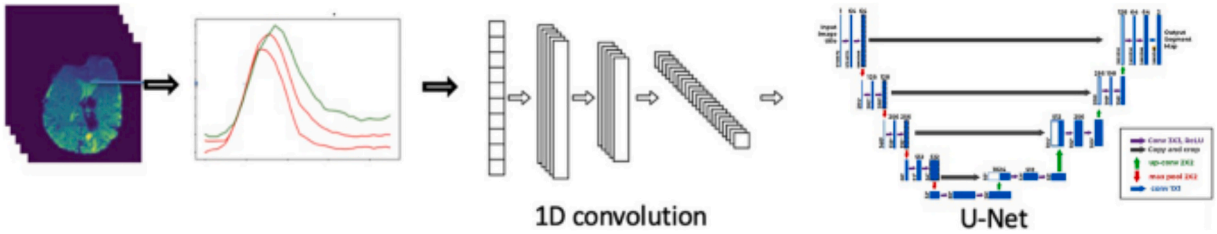

Fig. 4. Overview of the multistage encoder architecture followed by a decoder proposed by Talebi et al. to process the DSC-MRI datasets. The model captures temporal features followed by a modified U-net to generate the perfusion maps. Figure from Talebi et al., 2024, Ann Biom Eng, 52(6), 1568–75, under the Creative Commons license (CC-BY 4.0) [55].

data and a network layer. A main advantage is their time invariance with respect to time shift. A critical aspect of these networks, i.e. problems related to vanishing or exploding gradients, could be solved if the LSTM nets are adopted, resulting in good performance of CBV estimation, as shown in an exemplificative case.

Similarly to other perfusion techniques, also for DSC-MRI physics-informed neural networks have been proposed to estimate perfusion parameters without the need of external training data. ANN architectures based on multi-layer perceptron were developed, trained using a physics-informed loss function [24,57] on simulated data and evaluated on in-vivo patients. Cao et al. replaced ANN with a CNN that considered spatio-temporal information of the DSC-MRI acquisitions [58]. In all these studies, physics-informed DL approaches were able to provide an accurate estimate of perfusion coefficients, thus overcoming the ill-pose mathematical problem of solving deconvolution with traditional regularization methods. Specifically, physics-informed ANNs and CNNs presented high correlations between conventionally derived and DL-predicted perfusion parameters (Pearson's rho for CBF: 0.84 ± 0.03 and CBV: 0.92 ± 0.03) and very high indices of image similarity (SSIM greater than 0.9) [57,58].

4.3. ASL-MRI

With the advent of DL techniques, novel strategies have been proposed for the estimation of perfusion parameters from ASL acquisitions (see Table 3). Ishida et al. firstly proposed an ANN for the estimation of CBF and ATT from multi-delay ASL using both a supervised [59] and a physics-informed unsupervised learning (Fig. 5) [60]. The authors reported that the physics-informed unsupervised ANNs demonstrated greater accuracy and noise resistance in perfusion parameter estimation compared to the traditional WD method and NLLS solution for estimating ATT and CBF. The supervised ANN exhibited superior accuracy in estimating both CBF and ATT and showed better noise resistance for CBF estimation. Conversely, the physics-informed unsupervised ANN showed better noise resistance in ATT estimation. While the accuracy of supervised learning is influenced only by the parameters being estimated, the accuracy of physics-informed unsupervised learning is affected by both CBF and ATT [60]. The comparison between supervised and physics-informed unsupervised ANN was evaluated also for the estimation of perfusion parameters in the Multiparametric-ASL acquisition, which enables the quantification of additional parameters pertinent to brain function, such as arterial cerebral blood volume (CBVa) and permeability-related parameters [61]. From this preliminary evaluation, which considered both simulated data and 8 healthy subjects, the supervised approach seems to provide the most accurate and precise results, with lower values for Normalized Root Mean Square Error (NRMSE), Normalized Mean Absolute Error (NMAE), and Coefficient of Variation (CV). In-vivo analysis also demonstrated satisfactory reproducibility for both supervised and unsupervised learning.

DL has demonstrated great improvements, especially in terms of computation time, for the quantification of perfusion parameters from MR fingerprinting (MRF) – based ASL. MRF-ASL is a recently developed

Table 3
List of papers proposing the use of DL approaches for ASL-MRI applications.

Task	Type of DL method	Data	Validation	Evaluation metrics	Code available	Ref
ASL quantification	ANN – Supervised	Simulations + 17 healthy brain subjects (retrospective)	Training on simulations, validation on simulations and in vivo data	NMAE and NRMSE lower than other approaches	No	[59]
ASL quantification	ANN – Unsupervised vs. supervised	Simulations + 17 healthy brain subjects	Internal by split	NMAE and NRMSE lower for supervised ANN than unsupervised	No	[60]
MP-ASL quantification	ANN – Supervised vs. physics-informed	Simulations + 8 healthy brain subjects	Training on simulations, validation on simulations and in vivo data	NMAE and NRMSE lower for supervised ANN than unsupervised	No	[61]
MRF-ASL quantification	ANN – Supervised	Simulations + 7 healthy and 3 pathologic brain subjects	Training on simulations, validation on simulations and in vivo data	ICC higher than conventional approaches	No	[64]
MRF-ASL quantification	ANN – Supervised	Simulations + 6 healthy brain subjects	On simulated digital objects and in vivo data	Correlation with ground truth data = 86.7 %	No	[65]
MRF-ASL quantification	ANN – Supervised	15 healthy brain subjects	Internal by split	Correlation with conventional approach between 0.84 and 0.96	No	[63]
Image reconstruction	CNN – Supervised	30 healthy brain subjects	5-fold cross-validation	PSNR = 22.13 dB SSIM = 0.56	No	[66]
Denoising	CNN Autoencoder – Supervised	131 pediatric neuro-oncologic patients + 11 healthy adults	Training on pediatric patients, testing on healthy adults	PSNR = 41 dB SSIM = 0.88	No	[67]
Denoising and reconstruction	3D Unet – Unsupervised	3 healthy brain subjects	Training on anatomical imaging, testing on ASL data	PSNR and SSIM significantly higher than other approaches	No	[68]

ANN: Artificial Neural Network; MP-ASL: Multiparametric ASL; MRF-ASL: MR fingerprinting-based ASL; CNN: Convolutional Neural Network; NMAE: Normalized Mean Absolute Error; NRMSE: Normalized Root Mean Square Error; ICC: Intraclass Correlation Coefficient; PSNR: Peak Signal-to-Noise Ratio; SSIM: Structural Similarity Index Measure.

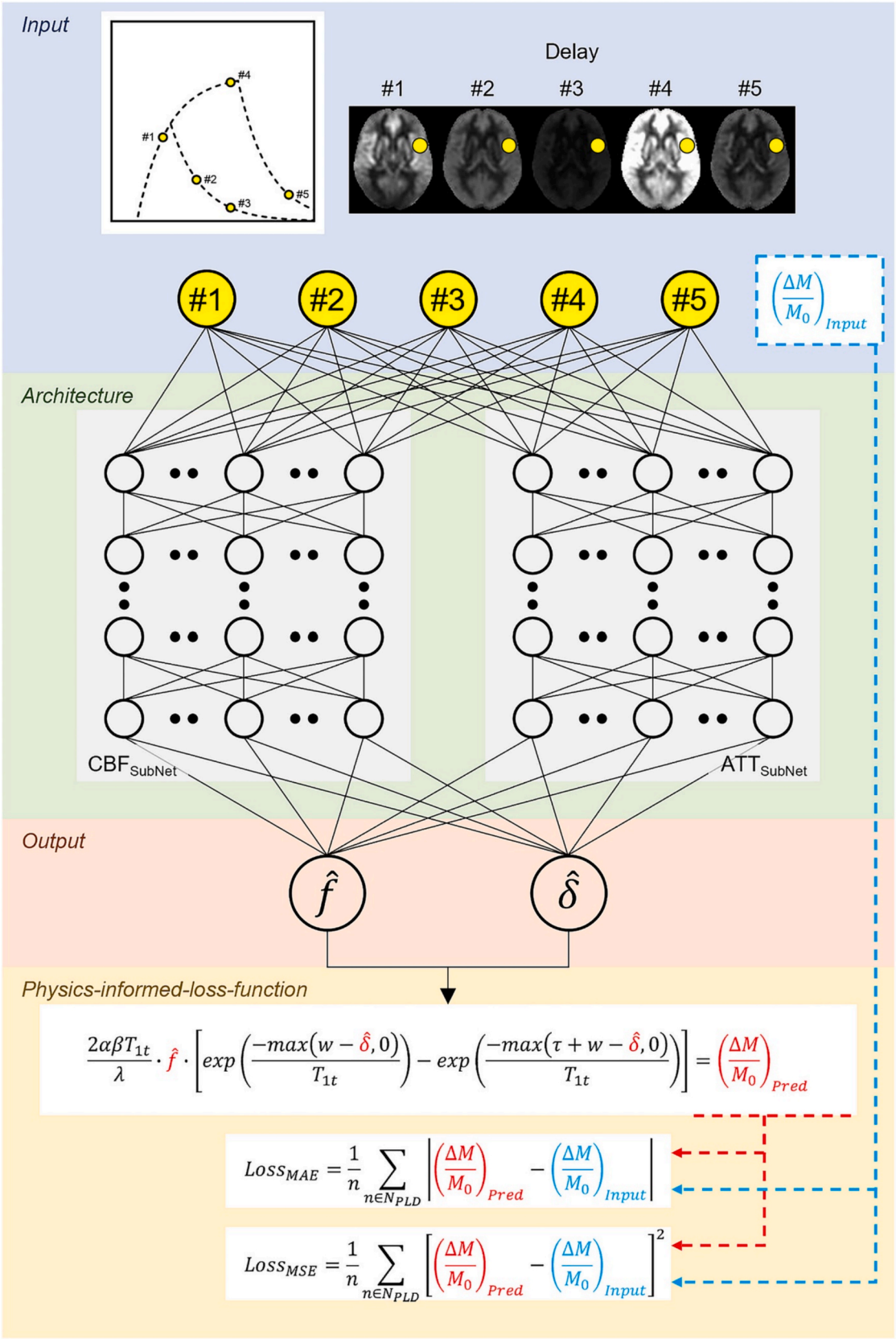

Fig. 5. Overview of training process and schematic diagram of the unsupervised network proposed by Ishida et al. First, a network consisting of two subnetworks simultaneously predicts CBF ($\hat{f}$) and ATT ($\hat{\delta}$) from the input signals. Subsequently, ASL signals are calculated using the single-compartment model with the predicted parameters. Finally, the consistency between the input and the predicted signals is evaluated using Mean Absolute Error (MAE) or Mean Squared Error (MSE) and minimized by the training process. Figure from Ishida et al., 2024, NMR in Biomed, e5177, under the Creative Commons license (CC-BY 4.0) [60].

technique that allows the simultaneous estimation of multiple perfusion parameters in a single scan [62]. MRF-ASL uses varying repetition times and randomized control/label sequences to uniquely encode different parameters in the MR signal. By matching experimental signals to a pre-generated dictionary, parameters such as CBF, Bolus Arrival Time (BAT), and tissue T_1 are assigned to voxels. However, the method has limitations, including modest reliability for parameter estimations when many parameters are involved, and high computational and storage demands for dictionary matching (up to 2 h for a single slice) [63]. ANNs have thus the potential to solve quantitative problems using a large number of highly interconnected processing nodes working together, not relying on analytical assumptions. Zhang et al. [64] and Lahiri et al. [65] assessed ANNs for this purpose, using simulated data for training and simulated digital objects and in-vivo data for validation, and provided faster and more accurate results than traditional approaches, as demonstrated by high Intraclass Correlation Coefficient (ICC) and correlation with ground truth data. A further study by Fan et al. overcame the limitations due to the use of simulations for training, which are not able to completely describe the complexity present in real voxels, by using a high-fidelity ANN trained and tested on 15 healthy subjects (5 for training, 5 for validation and 5 for testing) [63]. The authors reported that CV of high-fidelity ANN, traditional approach based on dictionary, and ANN trained on simulations was 0.15 ± 0.08, 0.41 ± 0.20, 0.30 ± 0.16, respectively, for CBF and 0.11 ± 0.06, 0.20 ± 0.19, 0.15 ± 0.10, respectively, for BAT.

DL has been suggested for a variety of applications beyond the direct estimation of ASL parameters, including the enhancement of image quality. This, in turn, can indirectly improve the assessment of ASL

Table 4
List of papers proposing the use of DL approaches for IVIM parameters quantification.

Task	Type of DL method	Data	Validation	Evaluation metrics	Code available	Ref
IVIM-DKI map quantification	ANN Supervised	Simulations + 7 brain healthy subjects	Training on simulations, validation on simulations and in vivo data	NRMSE < 10 % (*D*) NRMSE = 33.6 % (*f*) NRMSE = 26.8 % (*D**)	No	[77]
IVIM map quantification	ANN Unsupervised	Simulations + 10 healthy subjects (abdomen)	Training and validation on the same subjects + validation on simulations	0.5 < ICC < 0.97 9.2 < CV < 28.4 RMSE lower than other approaches	Yes	[78]
IVIM map quantification	ANN Unsupervised (physics-informed)	Simulations + 23 pancreatic cancer patients (retrospective)	Training on simulations, validation on simulations and in vivo data	NMRSE = 0.18 (*D*) NMRSE = 0.22 (*f*) NMRSE = 0.39 (*D**)	Yes	[79]
IVIM map quantification + b-value optimization	ANN Supervised	Simulations + 5 healthy brain subjects	Training on simulations, validation on simulations and in vivo data	NRMSE < 0.1 (*D*) NRMSE < 0.4 (*f*) NRMSE < 0.5 (*D**)	No	[81]
IVIM map quantification	ANN Supervised	Simulations + 1 mouse brain	Training on simulations, validation on simulations and in vivo data	MdAE < 0.2 (*D*) MdAE < 0.3 (*f*) MdAE < 0.4 (*D**)	No	[80]
Dynamic-exponential IVIM map quantification	ANN Unsupervised	Simulations + 10 hepatic healthy subjects (prospective)	Training on simulations, validation on simulations and in vivo data	RMSE lower than traditional approaches	Yes	[82]
Tri-exponential IVIM map quantification	ANN Unsupervised (physics-informed)	Simulations + 36 non-alcoholic fatty liver disease patients	Training on simulations, validation on simulations and in vivo data	RMSE lower than traditional approaches	No	[84]
IVIM map quantification	ANN Unsupervised + data consistency term	Simulations + 1 healthy subject + 38 fetal lungs	Training on simulations, validation on simulations and in vivo data	NMRSE lower than other DL approaches	Yes	[83]
IVIM map quantification	ANN Unsupervised vs. supervised	Simulations + 28 glioma patients (retrospective)	Training on simulations, validation on simulations and in vivo data	RMSE measured in different conditions and configurations	Yes	[85]
IVIM map quantification	CNN Self-supervised (physics-informed)	134 Pediatric Crohn's disease patients (retrospective)	Internal by split	NRMSE < 0.3 (*D*) NRMSE < 0.4 (*f*) NRMSE < 0.25 (*D**)	No	[86]
IVIM map quantification + classification	Transformer block to share information between tasks	114 Hepatocellular cancer patients (retrospective)	Nested 4-fold cross-validation	Accuracy = 79.21 % AUC = 85.51 % RMSE = 0.039 SSIM = 0.894	Yes	[88]
IVIM map quantification	CNN Unsupervised	Simulations + 6 healthy abdominal subjects (public dataset)	Training on simulations, validation on simulations and in vivo data	RMSE < 0.0004 (*D*) RMSE < 0.09 (*f*) RMSE < 0.02 (*D**)	No	[87]
IVIM −DKI map quantification + b-values registration	CNN − Inverse transformation + physics-based loss	21 healthy brain subjects	Internal by split	NRMSE = 0.03 (*D*) NRMSE = 0.097 (*f*) NRMSE = 0.346 (*D**)	Yes	[89]
IVIM map quantification	Supervised + discriminator to improve consistency	Simulations + 98 Hepatocellular cancer patients (retrospective)	Training on simulations, validation on simulations and in vivo data	NRMSE always lower than other approaches	Yes	[92]
IVIM + NODDI map quantification	Transformer-based encoder and sparsity-based decoder	27 normal pregnant women	Internal by split	MSE = $2.2\text{x}10^{-4}$ (*D*) MSE = $0.063\text{x}10^{-4}$ (*f*) MSE = 0.014 (*D**)	Yes	[90]
IVIM image reconstruction	CNN Denoising autoencoder	Brain phantom + 15 brain tumor patients (retrospective)	Validation on external dataset	Bland-Altman plots	No	[93]
IVIM map quantification	ANN vs. CNN vs. Transformer + different learning strategies	Simulations + 1 healthy brain subject	Training on simulations, validation on simulations and in vivo data	Percentage Errors lower for supervised training with attention models	Yes	[91]

ANN: Artificial Neural Network; CNN: Convolutional Neural Network; DKI: Diffusion Kurtosis Imaging; NODDI: Neurite Orientation Dispersion and Density Imaging; ICC: Intraclass Correlation Coefficient; CV: Coefficient of Variation; RMSE: Root Mean Square Error; MdAE: Median Absolute Error.

parameters. Indeed, ASL is challenged by a low SNR, low spatial resolution, and extensive acquisition time. However, these challenges can be mitigated through the application of CNNs, which have demonstrated the capability to produce images that are not only of high quality but also denoised and of higher resolution, thereby significantly enhancing the reconstructed images [66–68].

4.4. IVIM-MRI

IVIM model coefficients are traditionally estimated by fitting the bi-exponential signal decay using NLLS methods or Bayesian approaches [69]. With the last technique, it is possible to introduce homogeneity priors that allow to spatially regularize the estimated parametric maps during the fitting procedure directly [70–72]. The fitting accuracy depends on several factors, among which the estimation algorithm, the SNR level, and the amount of perfusion [73,74].

In the last few years DL has been introduced in the IVIM field as a valid alternative to traditional fitting methods. DL-based IVIM quantification seems not only to improve the accuracy in parameters estimation, but also to better preserve the texture information of the different tissues, compared to NLLS and Bayesian methods [75]. Two main approaches have been proposed to obtain quantitative parametric maps: i) a voxel-wise estimation, where a relatively compact ANN predicts IVIM coefficients voxel-by-voxel, and ii) the adoption of CNNs to estimate quantitative maps by considering spatial relationship between voxels and thus predict multiple voxels simultaneously [76]. In Table 4 a schematic representation of the works that proposed DL for IVIM parameter quantification is reported.

The first attempt to use ANN for IVIM-Kurtosis model quantification proposed a simple neural network with one hidden layer, that was trained in a supervised way using simulated data, obtaining an accuracy comparable to state-of-the-art methods (NRMSE = 0.1, 0.33, 0.27 for D, f and D*, respectively) [77]. Then, other groups proposed different implementations of ANNs to quantify IVIM model parameters voxel-by-voxel, with increasing improvements on accuracy and map quality [78–85]. An illustrative example is reported in Fig. 6. In some cases, the supervised approach was replaced by an unsupervised physics-informed loss, which did not require simulated data, that minimized the error between the original and the reconstructed MR signals [78,79,82,84]. However, Mastropietro et al. showed that the supervised approach, trained with a large number of simulated data, overcame the unsupervised technique, with average absolute error of 0.07 ± 0.04 for D, 0.14

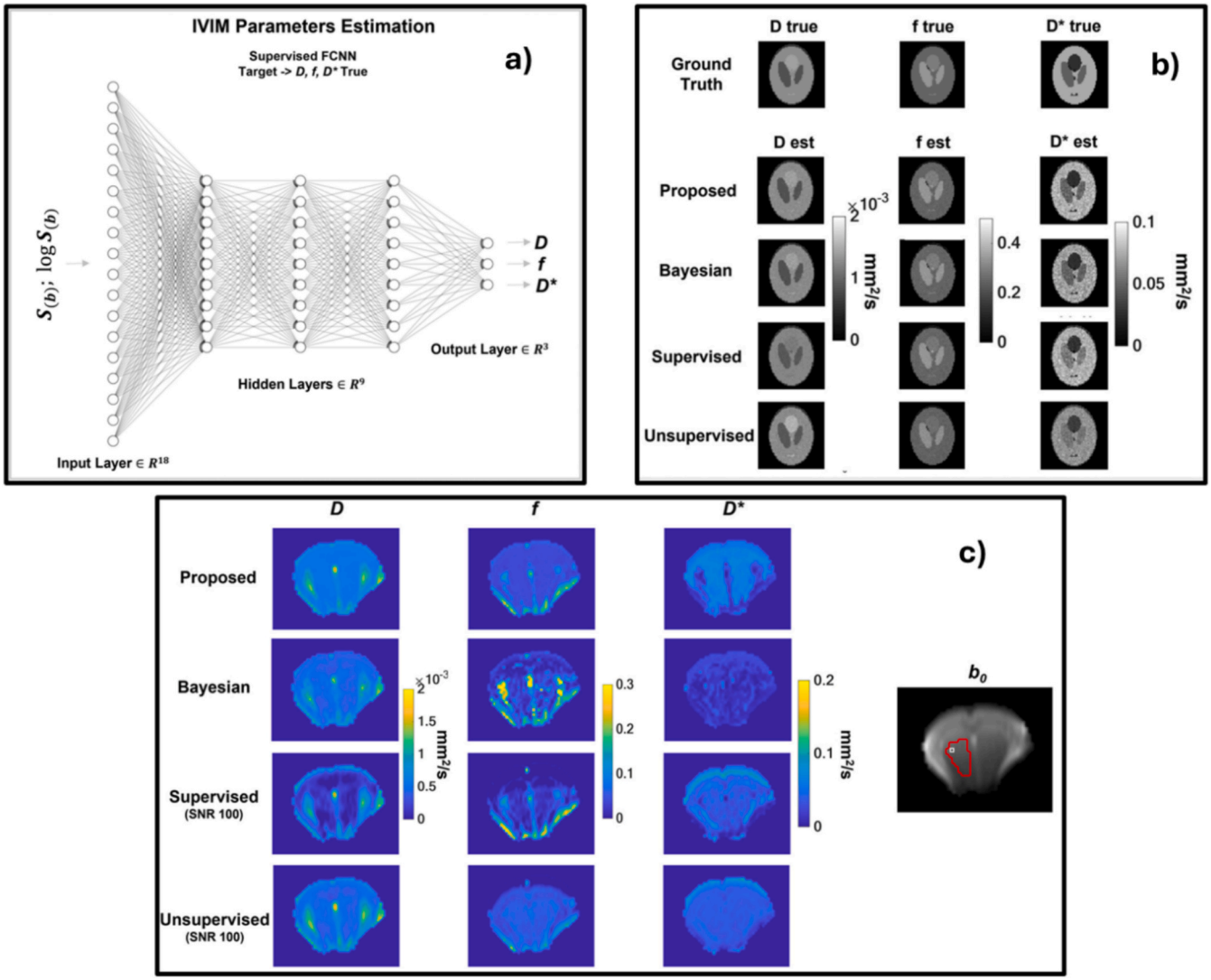

Fig. 6. Panel a): Overview of the ANN architecture proposed by Mastropietro et al., having three hidden layers, two b-value inputs and three standardized targets. Input data consist of the signal intensity values and their logarithm. Some examples of estimated parameter maps obtained using the proposed DNN approach and other implemented methods are displayed in panel b. Panel c): Evaluation of the proposed method, compared with the other implemented approaches, in a real preclinical scenario. Figure adapted from Mastropietro et al., 2022, NMR in Biomed, e4774, under the Creative Commons license (CC-BY 4.0) [80].

$\pm$ 0.08 for f and 0.26 $\pm$ 0.1 for D* [80]. Differences in learning strategies were assessed by Kaandorp et al., reporting that extensive training is required to minimize parameter correlation and bias for unsupervised training, whereas a close correspondence between the training and test sets is demanded for supervised learning [85]. Korngut et al. proposed a combined approach, where the loss function is a weighted sum of the error between estimated and reference IVIM coefficients and the error between reconstructed and original signal; this approach seems to reduce prediction errors compared to the unsupervised training, when a limited number of *b-values* are available [83]. The issue of the choice of the optimal *b-values* sampling was faced by Lee et al, who proposed an ANN that simultaneously optimized *b-values* scheme and model fitting, improving the performances compared to other traditional *b-values* optimization strategies, reporting NRMSE values lower than 0.1, 0.4 and 0.5 for D, f and D*, respectively [81]. They also found that the optimal choice of *b-values* for ANN depends on the SNR, which should thus be considered when DL approaches are designed.

More recently, CNNs have been proposed to capture the spatial dependency between neighboring voxels to effectively denoise the low SNR DW-MRI signal data, using a self-supervised training approach, based on physics-informed loss function [86,87]. One of the main advantages of CNNs is that they can be used for multiple tasks, that can also improve the accuracy in parameter estimation. For example, map quantification has been coupled with classification task [88] using transformer blocks to share knowledge between the two tasks, or with *b-values* registration [89], without the need of ground truth labels. In the first case, the multi-task DL network, trained and tested on 114 hepatocellular cancer patients, allowed the quantification of IVIM parametric maps with a RMSE of 0.039, and the prediction of microvascular invasion with accuracy of 79 % and AUC of 85 %, showing higher performances compared to single-task methods.

The use of transformers has been also proposed in a recent work to estimate parametric maps from IVIM and Neurite Orientation Dispersion and Density Imaging (NODDI) acquisitions [90]. Specifically, a transformer-based encoder has been adapted for model estimation task, followed by a sparsity-based decoder, able to introduce prior information related to the microstructural model of interest (IVIM or NODDI). This approach, tested on fetal MRI scans from normal pregnant women, showed high accuracy, good interpretability, high generalizability and robustness, compared to traditional methods and state-of-the-art learning-based techniques. Another study has explored the integration of spatial information into DL-based IVIM parameter estimation using transformers, evaluated within both supervised and self-supervised learning frameworks and across ANN and CNN architectures [91]. The underlying hypothesis was that attention mechanisms in transformers could effectively capture spatial dependencies by training on synthetic data with predefined neighbor correlations, ultimately surpassing traditional model-fitting methods. The findings demonstrated that incorporating attention models into supervised training led to significant improvements in accuracy compared to conventional voxel-wise and convolutional-based approaches.

Finally, the use of synthetic data to train the CNN in a supervised way was proposed by Huang et al. in combination with a discriminator to perform domain adaptation from the synthetic to the real domain to make the results less dependent from the parameter distribution of specific tissues, and thus more generalizable [92]. This method showed improved accuracy in presence of noise and artifacts, compared to traditional approaches and other ANN and CNN techniques.

Similarly to the other perfusion MRI techniques, CNNs have been used also to improve image quality in IVIM acquisitions. Through the use of a pre-trained denoising autoencoder, Hanamatsu et al. showed that the use of DL for DW-MRI image reconstruction had a stronger effect on higher *b-values*. The impact on IVIM coefficients estimation is larger on *f* and *D** than on *D* and *ADC* [93].

5. Discussion

This review has highlighted the enormous potential of DL in enhancing the analysis of perfusion MRI techniques such as DCE, DSC, ASL, and IVIM. The findings presented demonstrate that DL-based methods can provide faster and more accurate parameter estimation, offering significant advancements over traditional approaches. These advancements may revolutionize the field of perfusion MRI by addressing current challenges in both research and clinical applications.

5.1. Deep learning approaches for perfusion MRI

In terms of DL approaches, ANNs, CNNs and RNNs have emerged as the most widely adopted methods for assessing perfusion MRI parameters across different modalities.

1. DCE-MRI has seen significant advancements with the application of CNNs and ANNs for PK model fitting. CNNs have been employed to estimate PK parameters more rapidly and accurately compared to traditional methods, particularly in cancer and stroke imaging. For instance, CNNs have been used to improve the estimation of tissue parameters such as K^{trans} (the transfer constant) by directly learning from time-series data without requiring manual input for AIF. Additionally, RNNs have shown promising results in DCE-MRI for estimating PK parameters, particularly when dealing with noisy data or undersampled time-series, offering a faster and more efficient alternative to NLLS fitting.
2. DSC-MRI, primarily used in brain perfusion studies (e.g., stroke and tumor imaging), benefits significantly from DL approaches like bi-input CNNs and RNNs. CNNs have been successfully applied to bypass the need for deconvolution, a critical step in traditional DSC analysis that is prone to noise sensitivity. For example, Ho et al. used a CNN to estimate critical parameters like cerebral blood volume (CBV) and cerebral blood flow (CBF) directly from the signal, improving the reliability of salvageable brain tissue estimation during stroke [54]. RNNs, such as LSTMs, have also been effective in capturing the temporal dynamics of DSC data, enhancing the accuracy of perfusion parameter extraction across different clinical scenarios.
3. In ASL-MRI, which is a non-invasive method that measures CBF without the use of contrast agents, DL has been applied to overcome challenges related to low SNR and low spatial resolution. ANNs have been widely used to estimate CBF and ATT from ASL data, providing more noise-resistant and accurate results than traditional model-based approaches. Supervised and physics-informed unsupervised learning have both been employed to improve the quantification of ASL parameters, making the technique more robust in clinical applications such as monitoring neurodegenerative diseases.
4. IVIM-MRI, which is used to separate diffusion and perfusion effects in tissues, has benefitted from CNNs and ANNs for fitting bi-exponential models to the signal decay curves. ANN-based models have been applied in voxel-wise estimation of diffusion and perfusion coefficients (D, D*, and f), offering improved precision compared to traditional NLLS methods. CNNs have also been employed to denoise IVIM data and provide more reliable parametric maps, especially in low-SNR settings, by learning spatial correlations between neighboring voxels. This has proved particularly useful in applications such as liver and pancreatic cancer imaging, where IVIM is increasingly used for tissue characterization.

Overall, CNNs excel at capturing spatial features and are particularly effective for image segmentation, denoising, and parameter map generation, especially in DCE and DSC-MRI. ANNs and RNNs have demonstrated their strength in handling temporal and voxel-wise data, making them ideal for ASL and DCE applications where time-series analysis is crucial. GANs and U-Net architectures have also found

important roles in enhancing image quality and reducing noise in both DCE and IVIM MRI.

5.2. Clinical implications

Perfusion MRI can be highly relevant for certain clinical applications such as cancer diagnosis, stroke management, and neurovascular assessments. By automating the extraction of key perfusion parameters (e.g., cerebral blood flow, transfer constant, perfusion fractions, etc.), DL methods can accelerate the decision making process in clinical setting based on accurate data – capabilities especially crucial in time-sensitive settings like acute stroke [94] where fast and reliable identification of recoverable brain tissue can significantly improve outcomes.

Beyond performance gains, DL-based techniques enable novel clinical applications. Real-time or near-real-time analysis, thanks to the ability of DL approaches to estimate parameters with a reduced computational time compared to traditional approaches [64,65], can guide healthcare professionals during interventional procedures [95], providing immediate feedback on perfusion changes. In oncology, radiotherapy dose painting could leverage precise perfusion data to customize dose distribution within tumors. Although clinical trials on the use of DL approaches for parameters estimation in clinical applications have yet to be reported, most studies discussed in this review suggest a strong potential for DL-driven perfusion MRI to enable more timely and effective interventions across a broad range of conditions.

5.3. Challenges and limitations

Despite these promising advances, several limitations remain. The "black box" nature of many DL models, particularly in complex applications such as parameter estimation in perfusion MRI, continues to be a barrier to widespread clinical adoption. To enhance transparency, methods such as Class Activation Maps (CAMs) and feature visualization techniques have been developed [96]. These approaches elucidate the decision-making processes of DL models, thereby increasing clinician trust and facilitating clinical adoption

Additionally, the generalizability of DL models is often constrained by the quantity and variety of the training datasets. For example, models trained primarily on data from specific populations (e.g., brain tumor patients) may not perform as effectively when applied to other demographic groups or disease states. Usually, data augmentation techniques, such as rotation, scaling, and flipping of images, can artificially expand the amount of data composing the training datasets, thereby enhancing model robustness across different scenarios. More interestingly, in this context, DL approaches based on stable diffusion and text-guided diffusion model GLIDE [15,16] can have a relevant impact in the generation of synthetic datasets that can be used to expand data availability including realistic and high quality images.

Publicly available perfusion MRI datasets, such as QIN-BRAIN-DSC-MRI [97], Resting State Perfusion in Healthy Aging [98], and UCSF-PDGM [99], Liver-IVIM [100] provide valuable resources for researchers. Utilizing these datasets can aid in training models and can serve as reference data to compare different approaches. Nevertheless, the small amount of data and available applications usually limits their potential to improve generalizability. In this sense, enhancing generalizability would benefit from developing methods such as federated learning, which enables models to learn from data across multiple centers while preserving patient privacy.

Integrating DL models into perfusion MRI presents also challenges related to standardization, sequence sensitivity, and quality assurance. Variations in MRI acquisition protocols, such as differences in pulse sequences and imaging parameters, might significantly impact the performance of DL methodology. Standardizing these parameters across institutions is crucial to ensure consistent input data, thereby enhancing model reliability and facilitating broader clinical adoption [101]. Developing models robust to such variations incorporating sequence-invariant feature representations during model training could enhance robustness and can boost their effective application in diverse clinical settings [102]. Finally, ensuring consistent image quality is paramount for DL applications in MRI. In this context, using standardized phantoms allows for the assessment and calibration of MRI scanners, ensuring that images meet predefined quality criteria [103]. By addressing these factors—standardization of acquisition parameters, sensitivity to sequence variations, and rigorous quality assurance—the robustness and clinical applicability of DL models in perfusion MRI can be enhanced.

5.4. Future directions

Looking forward, several emerging DL approaches hold immense potential to further revolutionize the analysis of Perfusion MRI. Key among these are foundation models, attention-based DL architectures, and transformer models, which have already begun making significant impacts in other fields and are poised to contribute to advancements in medical imaging.

1. Foundation Models (FMs): FMs, such as those based on large-scale pretraining datasets, are highly scalable and can be adapted for multiple tasks with minimal fine-tuning [104]. A recent literature review [16] has shown how FMs, even those based on Large Language Models (e.g., GPT-like models in natural language processing), pre-trained on extensive datasets, can be fine-tuned for specific medical imaging tasks, enhancing versatility and performance. They can adapt to new tasks with minimal data through in-context learning, reducing the need for extensive retraining. While promising, their direct use in quantitative MRI (qMRI) parameter estimation remains an emerging area of research. Currently, there is a lack of published studies explicitly employing FMs for this purpose. Therefore, there's still a potential to be explored and exploited. Indeed in the context of qMRI, FMs pre-trained on vast amounts of diverse imaging data, including different MRI modalities and pathologies, could be fine-tuned for specific tasks such as perfusion parameter estimation. This approach could lead to more generalizable DL systems capable of handling a wider range of patient demographics and disease conditions without requiring extensive retraining for each new application. Moreover, the ability of FMs to incorporate multimodal data (e.g., combining imaging data with electronic health records) could provide more comprehensive insights into patient conditions, allowing for personalized treatment planning [105].
2. Attention-Based DL and Transformer Models: Attention mechanisms and transformer models have already revolutionized natural language processing and are now being adapted for various image processing tasks, including medical imaging [106–108]. In perfusion MRI, transformer models have the potential to outperform traditional convolutional architectures by allowing the network to focus on the most relevant parts of the image or time-series data. Vision transformers (ViTs), for example, can capture long-range dependencies in imaging data, making them especially useful for tasks like time-resolved DCE-MRI, where both spatial and temporal correlations need to be considered. Transformers' self-attention mechanism can weigh the importance of different parts of the time series or image, providing more accurate parameter estimates by focusing on key patterns that might otherwise be missed by conventional CNNs or RNNs. Preliminary studies are already present in the context of DCE-and IVIM-MRI, as presented in Section 4.1 and 4.4.
3. In DSC-MRI, where noisy data often hampers the extraction of perfusion parameters, attention-based DL could help filter out irrelevant information and focus on critical regions of the brain affected by stroke or tumors. The flexibility of transformer models also might allow them to be applied to multi-sequence MRI data, integrating information from various sequences to provide a more holistic understanding of tissue perfusion.

4. Hybrid Models: Combining the strengths of traditional scientific models with modern DL approaches is another promising avenue [109]. For example, physics-informed deep learning models, which incorporate knowledge of underlying biological processes (e.g., pharmacokinetics in DCE-MRI [110]), have already shown improved performance in parameter estimation by ensuring that the learned representations adhere to known physical principles [111]. These hybrid approaches can be further enhanced by integrating attention mechanisms, allowing the model to dynamically adjust its focus based on the complexity or variability of the data.
5. Explainability and Clinical Integration: As these advanced DL models become more prevalent, the need for improved explainability and clinical integration will become even more critical. One of the primary challenges with models like transformers and foundation models is their "black box" nature, which can make it difficult for clinicians to trust AI-generated predictions. Future research should focus on developing explainable AI (XAI) methods that can visualize the decision-making process of these models [112,113]. For example, attention maps generated by transformers could be used to highlight the regions of an MRI scan that most influenced the model's predictions, making it easier for clinicians to interpret the results and make informed decisions.
6. Federated Learning and Data Privacy: As these new DL approaches are increasingly data-hungry, the challenge of obtaining large and diverse datasets, maintaining at the same time data privacy, becomes more pressing [114]. Federated learning, which allows DL models to be trained across multiple institutions without sharing sensitive patient data, could be an essential solution to this problem [115,116]. By using federated learning, models could benefit from a vast amount of real-world data while still adhering to privacy regulations. This approach could significantly enhance the generalizability of foundation models and transformers in clinical settings, allowing them to adapt to a wide variety of patient populations.

In summary, the future of DL in Perfusion MRI lies in leveraging these advanced DL techniques to create more flexible, generalizable, and interpretable models. The integration of attention-based mechanisms, transformer architectures, and foundation models, combined with domain-specific knowledge and federated learning, promises to enhance both the accuracy and clinical utility of DL approaches in medical imaging.

6. Conclusion

The integration of DL into Perfusion MRI holds great potential to transform diagnostic imaging, offering increased accuracy and efficiency. While challenges related to data scarcity and variety, model transparency, and clinical integration remain, continued advancements in DL technologies, coupled with interdisciplinary collaboration, could lead to widespread adoption in clinical practice. As DL models continue to evolve, the goal of personalized, high-precision diagnostic imaging is becoming an increasingly attainable reality.

Declaration of competing interest

Dr. Nicola Bertolino is an employee of Charles River Laboratories. All the other authors declare that they have no known competing financial interests or personal relationships that could have appeared to influence the work reported in this paper.

References

[1] Jahng GH, Li KL, Ostergaard L, Calamante F. Perfusion magnetic resonance imaging: a comprehensive update on principles and techniques. Korean J Radiol 2014;15:554–77. https://doi.org/10.3348/KJR.2014.15.5.554.
[2] Ottens T, Barbieri S, Orton MR, Klaassen R, van Laarhoven HWM, Crezee H, et al. Deep learning DCE-MRI parameter estimation: Application in pancreatic cancer. Med Image Anal 2022;80:102512. https://doi.org/10.1016/J.MEDIA.2022.102512.
[3] Shalom ES, Khan A, Van Loo S, Sourbron SP. Current status in spatiotemporal analysis of contrast-based perfusion MRI. Magn Reson Med 2024;91:1136–48. https://doi.org/10.1002/MRM.29906.
[4] Choi KS. Deep learning applications in perfusion MRI: recent advances and current challenges. Investig Magn Reson Imaging 2022;26:246–55. https://doi.org/10.13104/imri.2022.26.4.246.
[5] Soun JE, Chow DS, Nagamine M, Takhtawala RS, Filippi CG, Yu W, et al. Artificial intelligence and acute stroke imaging. Am J Neuroradiol 2021;42:2–11. https://doi.org/10.3174/AJNR.A6883.
[6] Yedavalli VS, Tong E, Martin D, Yeom KW, Forkert ND. Artificial intelligence in stroke imaging: Current and future perspectives. Clin Imaging 2021;69:246–54. https://doi.org/10.1016/J.CLINIMAG.2020.09.005.
[7] Argentiero A, Muscogiuri G, Rabbat MG, Martini C, Soldato N, Basile P, et al. The applications of artificial intelligence in cardiovascular magnetic resonance—A comprehensive review. J Clin Med 2022;11:2866. https://doi.org/10.3390/JCM11102866.
[8] Currie G, Hawk KE, Rohren E, Vial A, Klein R. Machine learning and deep learning in medical imaging: intelligent imaging. J Med Imaging Radiat Sci 2019. https://doi.org/10.1016/j.jmir.2019.09.005.
[9] Lecun Y, Bengio Y, Hinton G. Deep learning. Nature 2015;521:436–44. https://doi.org/10.1038/nature14539.
[10] Schmidhuber J. Deep learning in neural networks: An overview. Neural Netw 2015;61:85–117. https://doi.org/10.1016/J.NEUNET.2014.09.003.
[11] Yamashita R, Nishio M, Do RKG, Togashi K. Convolutional neural networks: an overview and application in radiology. Insights Imaging 2018;9:611–29. https://doi.org/10.1007/S13244-018-0639-9/FIGURES/15.
[12] Ronneberger O, Fischer P, U-net BT. Convolutional networks for biomedical image segmentation. Lecture Notes in Computer Science (including subseries Lecture Notes in Artificial Intelligence and Lecture Notes in Bioinformatics) 2015; vol. 9351:234–41.
[13] Litjens G, Kooi T, Bejnordi BE, Setio AAA, Ciompi F, Ghafoorian M, et al. A survey on deep learning in medical image analysis. Med Image Anal 2017;42:60–88. https://doi.org/10.1016/j.media.2017.07.005.
[14] Goodfellow IJ, Pouget-Abadie J, Mirza M, Xu B, Warde-Farley D, Ozair S, et al. Generative adversarial nets. Adv Neural Inf Process Syst 2014;27:2672–80.
[15] Kather JN, Ghaffari Laleh N, Foersch S, Truhn D. Medical domain knowledge in domain-agnostic generative AI. NPJ Digit Med 2022;5(1):1–5. https://doi.org/10.1038/s41746-022-00634-5.
[16] Avanzo M, Stancanello J, Pirrone G, Drigo A, Retico A. The evolution of artificial intelligence in medical imaging: from computer science to machine and deep learning. Cancers (Basel) 2024;16:3702. https://doi.org/10.3390/cancers16213702.
[17] Hochreiter S, Schmidhuber J. Long short-term memory. Neural Comput 1997;9:1735–80. https://doi.org/10.1162/NECO.1997.9.8.1735.
[18] Chung J, Gulcehre C, Cho K, Bengio Y. Empirical Evaluation of Gated Recurrent Neural Networks on Sequence Modeling 2014. https://doi.org/10.48550/arXiv.1412.3555.
[19] Vaswani A, Brain G, Shazeer N, Parmar N, Uszkoreit J, Jones L, et al. Attention is all you need. Adv Neural Inf Process Syst 2017:30. https://doi.org/10.48550/arXiv.1706.03762.
[20] Khalifa F, Soliman A, El-Baz A, Abou El-Ghar M, El-Diasty T, Gimel'Farb G, et al. Models and methods for analyzing DCE-MRI: a review. Med Phys 2014;41(12):124301. https://doi.org/10.1118/1.4898202.
[21] Tofts PS, Brix G, Buckley DL, Evelhoch JL, Henderson E, Knopp MV, et al. Estimating kinetic parameters from dynamic contrast-enhanced T1- weighted MRI of a diffusable tracer: Standardized quantities and symbols. J Magn Reson Imaging 1999;10:223–32. https://doi.org/10.1002/(SICI)1522-2586(199909)10:3<223::AID-JMRI2>3.0.CO;2-S.
[22] Patlak CS, Blasberg RG, Fenstermacher JD. Graphical evaluation of blood-to-brain transfer constants from multiple-time uptake data. 1983;3:1–7. https://doi.org/10.1038/JCBFM.1983.1.
[23] Calamante F. Perfusion MRI using dynamic-susceptibility contrast MRI: Quantification issues in patient studies. Top Magn Reson Imaging 2010;21:75–85. https://doi.org/10.1097/RMR.0B013E31821E53F5.
[24] Asaduddin M, Kim EY, Park SH. SPINNED: Simulation-based physics-informed neural network for deconvolution of dynamic susceptibility contrast MRI perfusion data. Magn Reson Med 2024;92:1205–18. https://doi.org/10.1002/mrm.30095.
[25] McKinley R, Hung F, Wiest R, Liebeskind DS, Scalzo F. A machine learning approach to perfusion imaging with dynamic susceptibility contrast MR. Front Neurol 2018;9. https://doi.org/10.3389/fneur.2018.00717.
[26] Ferré JC, Bannier E, Raoult H, Mineur G, Carsin-Nicol B, Gauvrit JY. Arterial spin labeling (ASL) perfusion: Techniques and clinical use. Diagn Interv Imaging 2013;94:1211–23. https://doi.org/10.1016/J.DIII.2013.06.010.
[27] Iutaka T, de Freitas MB, Omar SS, Scortegagna FA, Nael K, Nunes RH, et al. arterial spin labeling: techniques, clinical applications, and interpretation. Radiographics 2023;43. https://doi.org/10.1148/RG.220088/ASSET/IMAGES/LARGE/RG.220088.FIG22.JPEG.
[28] Wang Z. Arterial spin labeling perfusion MRI signal processing through traditional methods and machine learning. Investig Magn Reson Imaging 2022;26:220. https://doi.org/10.13104/IMRI.2022.26.4.220.
[29] Alsop DC, Detre JA, Golay X, Günther M, Hendrikse J, Hernandez-Garcia L, et al. Recommended implementation of arterial spin-labeled perfusion MRI for clinical applications: A consensus of the ISMRM perfusion study group and the European

consortium for ASL in dementia. Magn Reson Med 2015;73:102–16. https://doi.org/10.1002/MRM.25197.
[30] Buxton RB, Frank LR, Wong EC, Siewert B, Warach S, Edelman RR. A general kinetic model for quantitative perfusion imaging with arterial spin labeling. Magn Reson Med 1998;40:383–96. https://doi.org/10.1002/MRM.1910400308.
[31] Petersen ET, Lim T, Golay X. Model-free arterial spin labeling quantification approach for perfusion MRI. Magn Reson Med 2006;55:219–32. https://doi.org/10.1002/mrm.20784.
[32] Le Bihan D, Breton E, Lallemand D, Grenier P, Cabanis E, Laval-Jeantet M. MR imaging of intravoxel incoherent motions: application to diffusion and perfusion in neurologic disorders. Radiology 1986;161:401–7. https://doi.org/10.1148/radiology.161.2.3763909.
[33] Hess A, Meier R, Kaesmacher J, Jung S, Scalzo F, Liebeskind D, et al. Synthetic perfusion maps: imaging perfusion deficits in DSC-MRI with deep learning. Lect Notes Comput Sci 2019;11383:447–55. https://doi.org/10.1007/978-3-030-11723-8_45/FIGURES/4.
[34] Dai W, Robson PM, Shankaranarayanan A, Alsop DC. Reduced resolution transit delay prescan for quantitative continuous arterial spin labeling perfusion imaging. Magn Reson Med 2012;67:1252–65. https://doi.org/10.1002/MRM.23103.
[35] Le Bihan D. What can we see with IVIM MRI? Neuroimage 2019;187:56–67. https://doi.org/10.1016/j.neuroimage.2017.12.062.
[36] Cho GY, Moy L, Zhang JL, Baete S, Lattanzi R, Moccaldi M, et al. Comparison of fitting methods and b-value sampling strategies for intravoxel incoherent motion in breast cancer. Magn Reson Med 2015;74:1077–85. https://doi.org/10.1002/mrm.25484.
[37] Jalnefjord O, Montelius M, Starck G, Ljungberg M. Optimization of b-value schemes for estimation of the diffusion coefficient and the perfusion fraction with segmented intravoxel incoherent motion model fitting. Magn Reson Med 2019;82:1541–52. https://doi.org/10.1002/mrm.27826.
[38] Lemke A, Stieltjes B, Schad LR, Laun FB. Toward an optimal distribution of b values for intravoxel incoherent motion imaging. Magn Reson Imaging 2011;29:766–76. https://doi.org/10.1016/j.mri.2011.03.004.
[39] Merisaari H, Jambor I. Optimization of b-value distribution for four mathematical models of prostate cancer diffusion-weighted imaging using b values up to 2000 s/mm2: Simulation and repeatability study. Magn Reson Med 2015;73:1954–69. https://doi.org/10.1002/mrm.25310.
[40] Klepaczko A, Strzelecki M, Kociołek M, Eikefjord E, Lundervold A. A multi-layer perceptron network for perfusion parameter estimation in DCE-MRI studies of the healthy kidney. Appl Sci (Switzerland) 2020;10. https://doi.org/10.3390/app10165525.
[41] Ulas C, Das D, Thrippleton MJ, Del Valdés Hernández MC, Armitage PA, Makin SD, et al. Convolutional neural networks for direct inference of pharmacokinetic parameters: application to stroke dynamic contrast-enhanced MRI. Front Neurol 2018;9:1147. https://doi.org/10.3389/fneur.2018.01147.
[42] Fang K, Wang Z, Li Z, Wang B, Han G, Cheng Z, et al. Convolutional neural network for accelerating the computation of the extended Tofts model in dynamic contrast-enhanced magnetic resonance imaging. J Magn Reson Imaging 2021;53:1898–910. https://doi.org/10.1002/jmri.27495.
[43] Kettelcamp J, Lingala SG. Arterial input function and tracer kinetic model-driven network for rapid inference of kinetic maps in Dynamic Contrast-Enhanced MRI (AIF-TK-net). In: 2020 IEEE 17th International Symposium on Biomedical Imaging (ISBI); 2020. p. 1450–3. https://doi.org/10.1109/ISBI45749.2020.9098349.
[44] Oh G, Moon Y, Moon WJ, Ye JC. Unpaired deep learning for pharmacokinetic parameter estimation from dynamic contrast-enhanced MRI without AIF measurements. Neuroimage 2024;291:120571. https://doi.org/10.1016/J.NEUROIMAGE.2024.120571.
[45] Bliesener Y, Acharya J, Nayak KS. Efficient DCE-MRI parameter and uncertainty estimation using a neural network. IEEE Trans Med Imaging 2020;39:1712–23. https://doi.org/10.1109/TMI.2019.2953901.
[46] Rastogi A, Dutta A, Yalavarthy PK. VTDCE-Net: A time invariant deep neural network for direct estimation of pharmacokinetic parameters from undersampled DCE MRI data. Med Phys 2023;50:1560–72. https://doi.org/10.1002/mp.16081.
[47] Rastogi A, Yalavarthy PK. Greybox: A hybrid algorithm for direct estimation of tracer kinetic parameters from undersampled DCE-MRI data. Med Phys 2024;51:4838–58. https://doi.org/10.1002/mp.16935.
[48] Zou J, Balter JM, Cao Y. Estimation of pharmacokinetic parameters from DCE-MRI by extracting long and short time-dependent features using an LSTM network. Med Phys 2020;47:3447–57. https://doi.org/10.1002/mp.14222.
[49] Zhao K, Pang K, Hung ALY, Zheng H, Yan R, Sung K. A deep learning-based framework for highly accelerated prostate MR dispersion imaging. Cancers (Basel) 2024;16. https://doi.org/10.3390/cancers16172983.
[50] Choi KS, You SH, Han Y, Ye JC, Jeong B, Choi SH. Improving the reliability of pharmacokinetic parameters at dynamic contrast-enhanced MRI in astrocytomas: A deep learning approach. Radiology 2020;297:178–88. https://doi.org/10.1148/RADIOL.2020192763/ASSET/IMAGES/LARGE/RADIOL.2020192763.FIG6.JPEG.
[51] Nalepa J, Ribalta Lorenzo P, Marcinkiewicz M, Bobek-Billewicz B, Wawrzyniak P, Walczak M, et al. Fully-automated deep learning-powered system for DCE-MRI analysis of brain tumors. Artif Intell Med 2020;102:101769. https://doi.org/10.1016/J.ARTMED.2019.101769.
[52] Benou A, Veksler R, Friedman A, Riklin RT. Ensemble of expert deep neural networks for spatio-temporal denoising of contrast-enhanced MRI sequences. Med Image Anal 2017;42:145–59. https://doi.org/10.1016/J.MEDIA.2017.07.006.
[53] Shaul R, David I, Shitrit O, Riklin RT. Subsampled brain MRI reconstruction by generative adversarial neural networks. Med Image Anal 2020;65:101747. https://doi.org/10.1016/J.MEDIA.2020.101747.
[54] Ho KC, Scalzo F, Sarma KV, El-Saden S, Arnold CW. A temporal deep learning approach for MR perfusion parameter estimation in stroke. Proceedings - International Conference on Pattern Recognition 2016:1315–20. https://doi.org/10.1109/ICPR.2016.7899819.
[55] Talebi S, Gai S, Sossin A, Zhu V, Tong E, Mofrad MRK. Deep learning for perfusion cerebral blood flow (CBF) and volume (CBV) predictions and diagnostics. Ann Biomed Eng 2024;52:1568–75. https://doi.org/10.1007/s10439-024-03471-7.
[56] Rotkopf LT, Zhang KS, Tavakoli AA, Bonekamp D, Ziener CH, Schlemmer HP. Quantitative analysis of DCE and DSC-MRI: from kinetic modeling to deep learning. RoFo Fortschritte Auf Dem Gebiet Der Rontgenstrahlen Und Der Bildgebenden Verfahren 2022;194:975–82. https://doi.org/10.1055/a-1762-5854.
[57] Rotkopf LT, Ziener CH, von Knebel-Doeberitz N, Wolf SD, Hohmann A, Wick W, et al. A physics-informed deep learning framework for dynamic susceptibility contrast perfusion MRI. Med Phys 2024. https://doi.org/10.1002/mp.17415.
[58] Cao A, Le PY, Qie Z, Guo Y, Zaman A, Lu J, et al. Quantitative perfusion maps using a novelty spatiotemporal convolutional neural network. Proceedings - International Symposium on Biomedical Imaging, IEEE Computer Society; 2024. https://doi.org/10.1109/ISBI56570.2024.10635136.
[59] Ishida S, Isozaki M, Fujiwara Y, Takei N, Kanamoto M, Kimura H, et al. estimation of cerebral blood flow and arterial transit time from multi-delay arterial spin labeling MRI using a simulation-based supervised deep neural network. J Magn Reson Imaging 2023;57:1477–89. https://doi.org/10.1002/jmri.28433.
[60] Ishida S, Fujiwara Y, Takei N, Kimura H, Tsujikawa T. Comparison between supervised and physics-informed unsupervised deep neural networks for estimating cerebral perfusion using multi-delay arterial spin labeling MRI. NMR Biomed 2024;37(10):e5177.
[61] Ishida S, Fujiwara Y, Matta Y, Takei N, Kanamoto M, Kimura H, et al. Enhanced parameter estimation in multiparametric arterial spin labeling using artificial neural networks. Magn Reson Med 2024;92:2163–80. https://doi.org/10.1002/mrm.30184.
[62] Su P, Fan H, Liu P, Li Y, Qiao Y, Hua J, et al. MR fingerprinting ASL: Sequence characterization and comparison with dynamic susceptibility contrast (DSC) MRI. NMR Biomed 2020;33:e4202.
[63] Fan H, Su P, Huang J, Liu P, Lu H. Multi-band MR fingerprinting (MRF) ASL imaging using artificial-neural-network trained with high-fidelity experimental data. Magn Reson Med 2021;85:1974–85. https://doi.org/10.1002/mrm.28560.
[64] Zhang Q, Su P, Chen Z, Liao Y, Chen S, Guo R, et al. Deep learning–based MR fingerprinting ASL ReconStruction (DeepMARS). Magn Reson Med 2020;84:1024–34. https://doi.org/10.1002/mrm.28166.
[65] Lahiri A, Fessler JA, Hernandez-Garcia L. Optimizing MRF-ASL scan design for precise quantification of brain hemodynamics using neural network regression. Magn Reson Med 2020;83:1979–91. https://doi.org/10.1002/mrm.28051.
[66] Li Z, Liu Q, Li Y, Ge Q, Shang Y, Song D, et al. A two-stage multi-loss super-resolution network for arterial spin labeling magnetic resonance imaging. Lect Notes Comput Sci 2019;11766:12–20. https://doi.org/10.1007/978-3-030-32248-9_2/FIGURES/3.
[67] Hales PW, Pfeuffer J, Clark AC. Combined denoising and suppression of transient artifacts in arterial spin labeling MRI using deep learning. J Magn Reson Imaging 2020;52:1413–26. https://doi.org/10.1002/JMRI.27255.
[68] Gong K, Han P, El Fakhri G, Ma C, Li Q. Arterial spin labeling MR image denoising and reconstruction using unsupervised deep learning. NMR Biomed 2022;35. https://doi.org/10.1002/nbm.4224.
[69] Orton MR, Collins DJ, Koh D-M, Leach MO. Improved intravoxel incoherent motion analysis of diffusion weighted imaging by data driven Bayesian modeling. Magn Reson Med 2014;71:411–20. https://doi.org/10.1002/mrm.24649.
[70] Kurugol S, Freiman M, Afacan O, Perez-Rossello JM, Callahan MJ, Warfield SK. Spatially-constrained probability distribution model of incoherent motion (SPIM) for abdominal diffusion-weighted MRI. Med Image Anal 2016;32:173–83. https://doi.org/10.1016/j.media.2016.03.009.
[71] Lanzarone E, Mastropietro A, Scalco E, Vidiri A, Rizzo G. A novel bayesian approach with conditional autoregressive specification for intravoxel incoherent motion diffusion-weighted MRI. NMR Biomed 2020;33:e4201.
[72] Scalco E, Mastropietro A, Rizzo G, Lanzarone E. A clustering approach to improve IntraVoxel incoherent motion maps from DW-MRI using conditional auto-regressive bayesian model. Appl Sci (Switzerland) 2022;12:1907. https://doi.org/10.3390/app12041907.
[73] Scalco E, Mastropietro A, Bodini A, Marzi S, Rizzo G. A multi-variate framework to assess reliability and discrimination power of Bayesian estimation of Intravoxel Incoherent Motion parameters. Phys Med 2021;89:11–9. https://doi.org/10.1016/J.EJMP.2021.07.025.
[74] While PT. A comparative simulation study of bayesian fitting approaches to intravoxel incoherent motion modeling in diffusion-weighted MRI. Magn Reson Med 2017;78:2373–87. https://doi.org/10.1002/mrm.26598.
[75] Scalco E, Rizzo G, Mastropietro A. The quantification of IntraVoxel incoherent motion – MRI maps cannot preserve texture information: An evaluation based on simulated and in-vivo images. Comput Biol Med 2023;154:106495. https://doi.org/10.1016/J.COMPBIOMED.2022.106495.
[76] Gurney-Champion OJ, Landry G, Redalen KR, Thorwarth D. Potential of deep learning in quantitative magnetic resonance imaging for personalized radiotherapy. Semin Radiat Oncol 2022;32:377–88. https://doi.org/10.1016/J.SEMRADONC.2022.06.007.

[77] Bertleff M, Domsch S, Weingärtner S, Zapp J, O'Brien K, Barth M, et al. Diffusion parameter mapping with the combined intravoxel incoherent motion and kurtosis model using artificial neural networks at 3 T. NMR Biomed 2017;30:e3833.

[78] Barbieri S, Gurney-Champion OJ, Klaassen R, Thoeny HC. Deep learning how to fit an intravoxel incoherent motion model to diffusion-weighted MRI. Magn Reson Med 2020;83:312–21. https://doi.org/10.1002/mrm.27910.

[79] Kaandorp MPT, Barbieri S, Klaassen R, van Laarhoven HWM, Crezee H, While PT, et al. Improved unsupervised physics-informed deep learning for intravoxel incoherent motion modeling and evaluation in pancreatic cancer patients. Magn Reson Med 2021;86:2250–65. https://doi.org/10.1002/MRM.28852.

[80] Mastropietro A, Procissi D, Scalco E, Rizzo G, Bertolino N. A supervised deep neural network approach with standardized targets for enhanced accuracy of IVIM parameter estimation from multi-SNR images. NMR Biomed 2022;35(10): e4774.

[81] Lee W, Kim B, Park HW. Quantification of intravoxel incoherent motion with optimized b-values using deep neural network. Magn Reson Med 2021;86: 230–44. https://doi.org/10.1002/MRM.28708.

[82] Zhou XX, Wang XY, Liu EH, Zhang L, Zhang HX, Zhang XS, et al. An unsupervised deep learning approach for dynamic-exponential intravoxel incoherent motion MRI modeling and parameter estimation in the liver. J Magn Reson Imaging 2022;56:848–59. https://doi.org/10.1002/JMRI.28074.

[83] Korngut N, Rotman E, Afacan O, Kurugol S, Zaffrani-Reznikov Y, Nemirovsky-Rotman S, et al. SUPER-IVIM-DC: intra-voxel incoherent motion based fetal lung maturity assessment from limited DWI data using supervised learning coupled with data-consistency. Lect Notes Comput Sci 2022:743–52. https://doi.org/10.1007/978-3-031-16434-7_71/FIGURES/4.

[84] Troelstra MA, Van Dijk AM, Witjes JJ, Mak AL, Zwirs D, Runge JH, et al. Self-supervised neural network improves tri-exponential intravoxel incoherent motion model fitting compared to least-squares fitting in non-alcoholic fatty liver disease. Front Physiol 2022;13. https://doi.org/10.3389/fphys.2022.942495.

[85] Kaandorp MPT, Zijlstra F, Federau C, While PT. Deep learning intravoxel incoherent motion modeling: Exploring the impact of training features and learning strategies. Magn Reson Med 2023;90:312–28. https://doi.org/10.1002/mrm.29628.

[86] Vasylechko SD, Warfield SK, Afacan O, Kurugol S. Self-supervised IVIM DWI parameter estimation with a physics based forward model. Magn Reson Med 2022;87:904–14. https://doi.org/10.1002/mrm.28989.

[87] Huang HM. An unsupervised convolutional neural network method for estimation of intravoxel incoherent motion parameters. Phys Med Biol 2022;67. https://doi.org/10.1088/1361-6560/ac9a1f.

[88] Huang H, Liu B, Zhang L, Xu Y, Zhou W. Transformer based multi-task deep learning with intravoxel incoherent motion model fitting for microvascular invasion prediction of hepatocellular carcinoma. Lecture Notes in Computer Science (Including Subseries Lecture Notes in Artificial Intelligence and Lecture Notes in Bioinformatics) 2022;13437 LNCS:266–75. https://doi.org/10.1007/978-3-031-16449-1_26/TABLES/2.

[89] Lee W, Choi G, Lee J, Park HW. Registration and quantification network (RQnet) for IVIM-DKI analysis in MRI. Magn Reson Med 2023;89:250–61. https://doi.org/10.1002/MRM.29454.

[90] Zheng T, Yan G, Li H, Zheng W, Shi W, Zhang Y, et al. A microstructure estimation Transformer inspired by sparse representation for diffusion MRI. Med Image Anal 2023;86:102788. https://doi.org/10.1016/J.MEDIA.2023.102788.

[91] Kaandorp MP, Zijlstra F, Karimi D, Gholipour A, While PT. Incorporating spatial information in deep learning parameter estimation with application to the intravoxel incoherent motion model in diffusion-weighted MRI. Med Image Anal 2025;101. https://doi.org/10.1016/j.media.2024.103414.

[92] Huang H, Liu B, Xu Y, Zhou W. Synthetic-to-real domain adaptation with deep learning for fitting the intravoxel incoherent motion model of diffusion-weighted imaging. Med Phys 2023;50:1614–22. https://doi.org/10.1002/MP.16031.

[93] Hanamatsu S, Murayama K, Ohno Y, Yamamoto K, Yui M, Toyama H. Deep learning reconstruction for brain diffusion-weighted imaging: efficacy for image quality improvement, apparent diffusion coefficient assessment, and intravoxel incoherent motion evaluation in in vitro and in vivo studies. Diagn Interv Radiol 2023;29:664–73. https://doi.org/10.4274/dir.2023.232149.

[94] Copen WA, Schaefer PW, Wu O. MR perfusion imaging in acute ischemic stroke. Neuroimaging Clin N Am 2011;21:259–83. https://doi.org/10.1016/J.NIC.2011.02.007.

[95] Nayak KS, Lim Y, Campbell-Washburn AE, Steeden J. Real-time magnetic resonance imaging. J Magn Reson Imaging 2022;55:81–99. https://doi.org/10.1002/JMRI.27411.

[96] Singh A, Sengupta S, Lakshminarayanan V. Explainable deep learning models in medical image analysis. J Imaging 2020;6:52. https://doi.org/10.3390/JIMAGING6060052.

[97] Schmainda KM, Prah MA, Connelly JM, Rand SD. Glioma DSC-MRI perfusion data with standard imaging and ROIs [Dataset] 2016. https://doi.org/10.7937/K9/TCIA.2016.5DI84Js8.

[98] Galiano A, Garcia de Eulate R, Vidorreta M, Recio M, Riverol M, Zubieta JL, et al. Resting state perfusion in healthy aging - OpenNeuro 2021. https://doi.org/10.18112/openneuro.ds000240.v2.0.0.

[99] Calabrese E, Villanueva-Meyer J, Rudie J, Rauschecker A, Baid U, Bakas S, et al. The University of California San Francisco Preoperative Diffuse Glioma MRI (UCSF-PDGM) (Version 4) . 2022. https://doi.org/10.7937/tcia.bdgf-8v37.

[100] Kovač JD, Daković M, Janković A, Mitrović M, Dugalić V, Galun D, et al. The role of intravoxel incoherent motion (IVIM) parameters in characterization of hypovascular liver lesions: the raw diffusion weighted images and IVIM data. Dataset: Dryad; 2020.

[101] Li XT, Huang RY. Standardization of imaging methods for machine learning in neuro-oncology. iv49 –55 Neurooncol Adv 2020;2. https://doi.org/10.1093/NOAJNL/VDAA054.

[102] Hu Z, Chen Z, Cao T, Lee HL, Xie Y, Li D, et al. Generalizable, sequence-invariant deep learning image reconstruction for subspace-constrained quantitative MRI. Magn Reson Med 2025. https://doi.org/10.1002/MRM.30433.

[103] Price RR, Axel L, Morgan T, Newman R, Perman W, Schneiders N, et al. Quality assurance methods and phantoms for magnetic resonance imaging: report of AAPM Nuclear Magnetic Resonance Task Group No. 1. Med Phys 1990;17(2): 287–95. https://doi.org/10.1118/1.596566.

[104] Azad B, Azad R, Eskandari S, Bozorgpour A, Kazerouni A, Rekik I, et al. Foundational models in medical imaging: a comprehensive survey and future vision 2023. https://doi.org/10.48550/arXiv.2310.18689.

[105] Zhang S, Metaxas D. On the challenges and perspectives of foundation models for medical image analysis. Med Image Anal 2024;91:102996. https://doi.org/10.1016/J.MEDIA.2023.102996.

[106] Shamshad F, Khan S, Zamir SW, Khan MH, Hayat M, Khan FS, et al. Transformers in medical imaging: A survey. Med Image Anal 2023;88:102802. https://doi.org/10.1016/j.media.2023.102802.

[107] He K, Gan C, Li Z, Rekik I, Yin Z, Ji W, et al. Transformers in medical image analysis. Intelligent Medicine 2023;3:59–78. https://doi.org/10.1016/J.IMED.2022.07.002.

[108] Hayat M, Aramvith S. Transformer's role in brain MRI: a scoping review. IEEE Access 2024;12:108876–96. https://doi.org/10.1109/ACCESS.2024.3434714.

[109] Sahu H, Kashyap R, Dewangan BK. Hybrid deep learning based semi-supervised model for medical imaging. 2022 OPJU International Technology Conference on Emerging Technologies for Sustainable Development, OTCON 2022 2023. https://doi.org/10.1109/OTCON56053.2023.10113904.

[110] Sainz-DeMena D, Pérez MA, García-Aznar JM. Exploring the potential of Physics-Informed Neural Networks to extract vascularization data from DCE-MRI in the presence of diffusion. Med Eng Phys 2024;123:104092. https://doi.org/10.1016/J.MEDENGPHY.2023.104092.

[111] Banerjee C, Nguyen K, Salvado O, Tran T, Fookes C. PINNs for Medical Image Analysis: A Survey 2024. https://doi.org/10.48550/arXiv.2408.01026.

[112] Borys K, Schmitt YA, Nauta M, Seifert C, Krämer N, Friedrich CM, et al. Explainable AI in medical imaging: An overview for clinical practitioners – Beyond saliency-based XAI approaches. Eur J Radiol 2023;162:110786. https://doi.org/10.1016/J.EJRAD.2023.110786.

[113] Qian J, Li H, Wang J, He L. Recent Advances in Explainable Artificial Intelligence for Magnetic Resonance Imaging. Diagnostics 2023;13:1571. https://doi.org/10.3390/DIAGNOSTICS13091571.

[114] Ziller A, Mueller TT, Stieger S, Feiner LF, Brandt J, Braren R, et al. Reconciling privacy and accuracy in AI for medical imaging. Nature Mach Intell 2024;6: 764–74. https://doi.org/10.1038/s42256-024-00858-y.

[115] Guan H, Yap PT, Bozoki A, Liu M. Federated learning for medical image analysis: A survey. Pattern Recognit 2024;151:110424. https://doi.org/10.1016/J.PATCOG.2024.110424.

[116] Rehman MHU, Hugo Lopez Pinaya W, Nachev P, Teo JT, Cardoso MJ. Federated learning for medical imaging radiology. Br J Radiol 2023;96. https://doi.org/10.1259/BJR.20220890/7498927.